CHAPTER 4

RESULTS AND DISCUSSION

The perovskite membrane used in partial oxidation of methane to syngas should possess a high electronic and ionic conductivity, high oxygen permeability, chemical stability, and a stable lattice structure for oxygen permeability over the used range of oxygen partial pressure. Several ABO_3-based perovskites, where La or Ba was in A site and Co or Ga was in B site of the cubic structure, had been reported to have those appropriate property. However, all these perovskites were prepared by the methods other than the modified citrate method [9, 12, 13].

The aim of this research is to prepare the perovskites by the modified citrate method. The synthesis and characterization of several ABO_3-based perovskites in powder forms were performed first. They were then cast into membranes. The membranes with only single-phase structure were selected for oxygen permeation testing.

In the following discussion, each perovskite compound is indicated by the abbreviation using the initial letters of each metal in A and B sites sequentially, followed by the corresponding number which refers to the proportion of each metal in the compound. For examples, $La_{0.8}Sr_{0.2}Ga_{0.4}Fe_{0.6}O_{3-\delta}$ and $La_{0.6}Sr_{0.4}Ga_{0.2}Fe_{0.8}O_{3-\delta}$ are abbreviated as LSGF8246 and LSGF6428, respectively. Similarly, $SrCo_{0.8}Fe_{0.2}O_{3-\delta}$, $La_{0.2}Ba_{0.8}Co_{0.2}Fe_{0.8}O_{3-\delta}$, $Ba_{0.5}Sr_{0.5}Ga_{0.2}Fe_{0.8}O_{3-\delta}$, and $Ba_{0.5}Sr_{0.5}Ga_{0.1}Co_{0.1}Fe_{0.8}O_{3-\delta}$ are abbreviated as SCF1082, LBCF2828, BSGF5528, and BSGCF55118, respectively.

4.1 Designation of Synthesized ABO_3-based Perovskites

The designation of ABO_3-based perovskites synthesized in this research was based on the thorough literature reviews. Eight types of ABO_3-based perovskites, as shown in Table 4.1, were selected for synthesis by modified citrate method and characterized mainly by XRD. These perovskites had tolerance number close to 1.00, which meant that they all should have a cubic structure.

Table 4.1 The selected ABO_3-based perovskites and the tolerance number

Compounds	Tolerance No.
SCF 1082	0.99
LSCF 2828	1.01
LBCF 2828	1.06
LSCF6428	1.00
LSGF 6428	1.01
BSCF5528	1.05
BSGF5528	1.05
BSGCF55118	1.03

The equation for the formation of these perovskites assuming complete combustion of the redox mixtures containing citric acid, for example, LSGF, can be written as;

$$(1\text{-}x)La(NO_3)_3 + xSr(NO_3)_2 + (1\text{-}y)Ga(NO_3)_3 + yFe(NO_3)_3 + 2HOC(COOH)(CH_2COOH)_2$$

$x = y = 0.2\text{-}0.8$

$$\downarrow$$

$$La_{1-x}Sr_xGa_{1-y}Fe_yO_{3-\delta}\,(s) + 12CO_2\,(g) + 8H_2O\,(g) + 3N_2\,(g) \qquad (19)$$

According to Equation (19), two moles of citric acid are required to react with 2 moles of all combined metal nitrates. In other words, the total metals will react with citric acid in the approximately equimolar ratio. However, in practice, the excess amount of citric acid was used to ensure the complete reaction of all the metal nitrates. Normally, three moles of citric acid were used to react with 2 moles of the total metal nitrates. Therefore, every three molecules of citric acid originally present, one remained uncombined and was removed from the mixture later by either evaporation or decomposition to yield carbon dioxide and water during heating in the vacuum oven [81]. In this research, the citric acid twice as much as the total metal nitrate was used in the synthesis of each perovskite.

4.2 Preliminary Study on the Synthesis of Perovskite Powder

In this preliminary study, the synthesis of $SrCoO_3$, $LaCoO_3$, $LaBaO_3$, and $BaFeO_3$-based perovskite was attempted by the modified citrate method. The synthesis conditions of all perovskites are shown in Table 3.2.

4.2.1 $SrCoO_{3-\delta}$ and $LaCoO_3$-based Perovskite

Teraoka et al. [87] were the first research groups to report that the very high oxygen-permeation flux was obtained through SCF1082 membrane. Attracted by its high permeability, the property of SCF1082 was re-examined by several other investigators [37, 88]. It was found that the material had very limited chemical and structural stability at lower oxygen partial pressure, especially in a reduced environment. In order to stabilize the phase stability of such material, Fe in SCF1082 was replaced by other metal ions, such as Cr, Mn, Fe, Ni, Cu and Ti. However, the oxygen permeation fluxs through those membranes were all greatly decreased.

$La_{1-x}A_xCo_{1-y}B_yO_{3-\delta}$ (A = Sr, Ba, Ca and B = Fe, Cu, Ni) perovskites were known to be highly oxygen anion defective at elevated temperatures and reduced oxygen partial pressure. The atomic ratio of Fe to Co in the B site of the perovskites was designated to be four, which gave a stable perovskite framework and allowed higher low-valent cation substitution in the A site to attain the desired property of high oxygen permeation flux [56]. Accordingly, SCF1082 and LSCF2828 were selected to be synthesized by modified citrate method and their XRD were investigated.

In the XRD analysis, the shape and size of the unit cell determines the angular positions of the diffraction lines (peaks), and the arrangement of the atoms within the unit cell determines the relative intensities of the lines. The single-phase perovskite with a cubic structure would exhibit the diffraction lines at the reflective planes 100, 110, 111, 200, 210, 211, and 220. The appearance of the splitting peaks indicates the distortion from the cubic structure and the presence of the diffraction lines other than those are due to the other compound or secondary phase.

The XRD patterns of SCF1082 and LSCF2828 calcined at 1,030°C were shown in Figure 4.1.

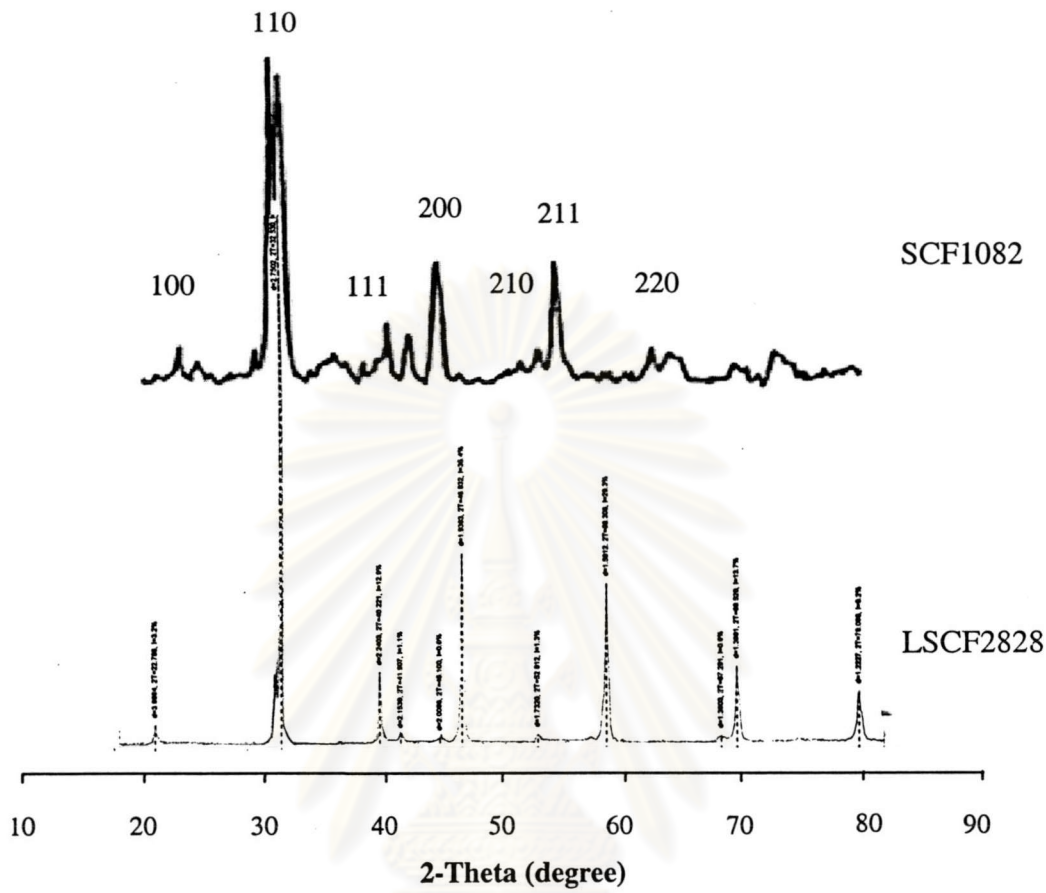

Figure 4.1 XRD patterns of SCF1082 and LSCF2828 perovskites calcined at 1,030°C for 5 hours

Based on the XRD analysis, SCF1082 had the cubic and distorted-cubic structure. This was due to the perovskite having the diffraction lines 100, 110, 111, 200, 210, 211, and 220, and having the spitting peak 110 at 2Θ = 32 degree. For LSCF2828, the XRD patterns showed mainly a cubic structure and trace amount of secondary phase, which was the peak at 2Θ = 30 degree. The unknown peaks in both compounds could not be identified at this stage due to the lack of the standard compound for comparison. However, by the XRD analysis, it clearly shows that the lanthanum in A site of ABO_3-based perovskite enhances the formation of the single phase and the cubic structure of the cobalt-containing perovskite synthesized by the modified citrate method.

4.2.2 Phase Transformation of $LaBaO_3$-based Perovskite by Calcination Temperature

It has been known that Ba can be substituted in A site, several research groups had studied the synthesis of LBCF2828 [56, 89]. Teraoka et al. [89] prepared LBCF perovskites by dissolving the iron nitrate and the other metal acetates, evaporated and calcined at 850°C for 10 hours. They found that barium-containing perovskite with substitution in A-site, A′, had the highest oxygen permeation rate, i.e., A′ = Ba > Ca > Sr for $La_{0.6}A'_{0.4}Co_{0.8}Fe_{0.2}O_{3-\delta}$ and $Ba_{0.8} > Ba_{0.6} > Ca_{0.6} > Sr_{0.6}$ for $La_{1-x}A'_xCo_{0.2}Fe_{0.8}O_{3-\delta}$ membranes. For LBCF2828 membrane, the cubic structure was stable in air and in helium ($P_{O2} \sim 10^{-4.5}$ atm) streams at elevated temperature. The membrane showed 100% oxygen selectivity for separation of oxygen from air in a helium/air gradient with about 0.1 cm^3/cm^2.min of oxygen permeation flux. Consequently, LBCF2828 was synthesized by the modified citrate method in this work.

To investigate the phase transformation in LBCF2828, the uncalcined powder was calcined at different temperature in the range of 800-1,100°C. Figure 4.2 shows the effect of the calcination temperatures on the phase purity of LBCF2828.

It should be noticed that some of the uncalcined powder existed in a perovskite structure as shown by the diffraction lines 100, 110, 111, 200, 210, 211, and 220, at 2Θ = 22, 32, 40, 46, 52, 58, 67, and 72 degree. The powder calcined at 800°C exhibited more perovskite structure with a trace amount of $BaCO_3$ due to the apparent peak at 2Θ = 24 degree. As the calcination temperature increased, $BaCO_3$ impurity was decreased as revealed by the lower intensity of the peak at 2Θ = 24 degree. This was due to the decomposition of $BaCO_3$ to BaO and CO_2, which had been explained by Tasi et al. [56]. However, La_2O_3 peak at 2Θ = 30 degree was observed and its intensity increased with increasing temperature. Therefore, the calcination temperature could influence the formation of the secondary phase in LBCF2828 perovskite. Furthermore, the splitting peak appeared at 2Θ = 30 degree disappeared when it was calcined at 1,000°C. Accordingly, the single phase of LBCF2828 can be prepared by the modified citrate method, but the calcination temperature at 1,000°C shall be used in order to minimize the formation of $BaCO_3$ and La_2O_3 as well as to suppress the distortion of its cubic structure.

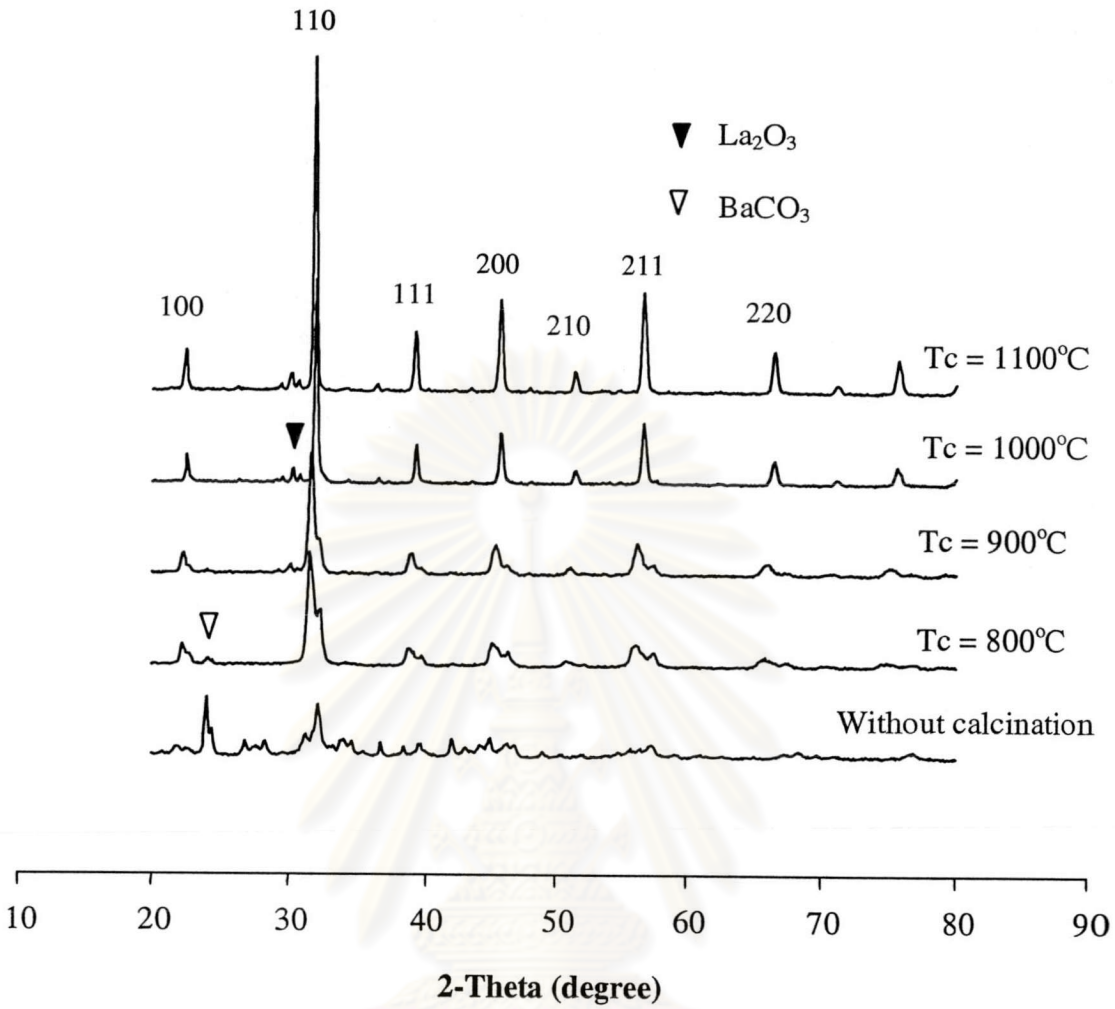

Figure 4.2 XRD patterns of LBCF2828 at different calcination temperature

4.2.3 The Influence of Synthetic Method on the Formation of $Ba_{0.5}Sr_{0.5}Ga_{0.1}Co_{0.1}Fe_{0.8}O_{3-\delta}$

BSGCF55118 was synthesized by two different methods, the modified citrate method and solid state method. In case of the solid state method, the equal amount of BSCF5528 and BSGF5528 was ground and thoroughly mixed, then calcined at 1,100°C for 5 hours to obtain the BSGCF55118. Figure 4.3 exhibited the XRD patterns of BSGCF55118 synthesized by both methods.

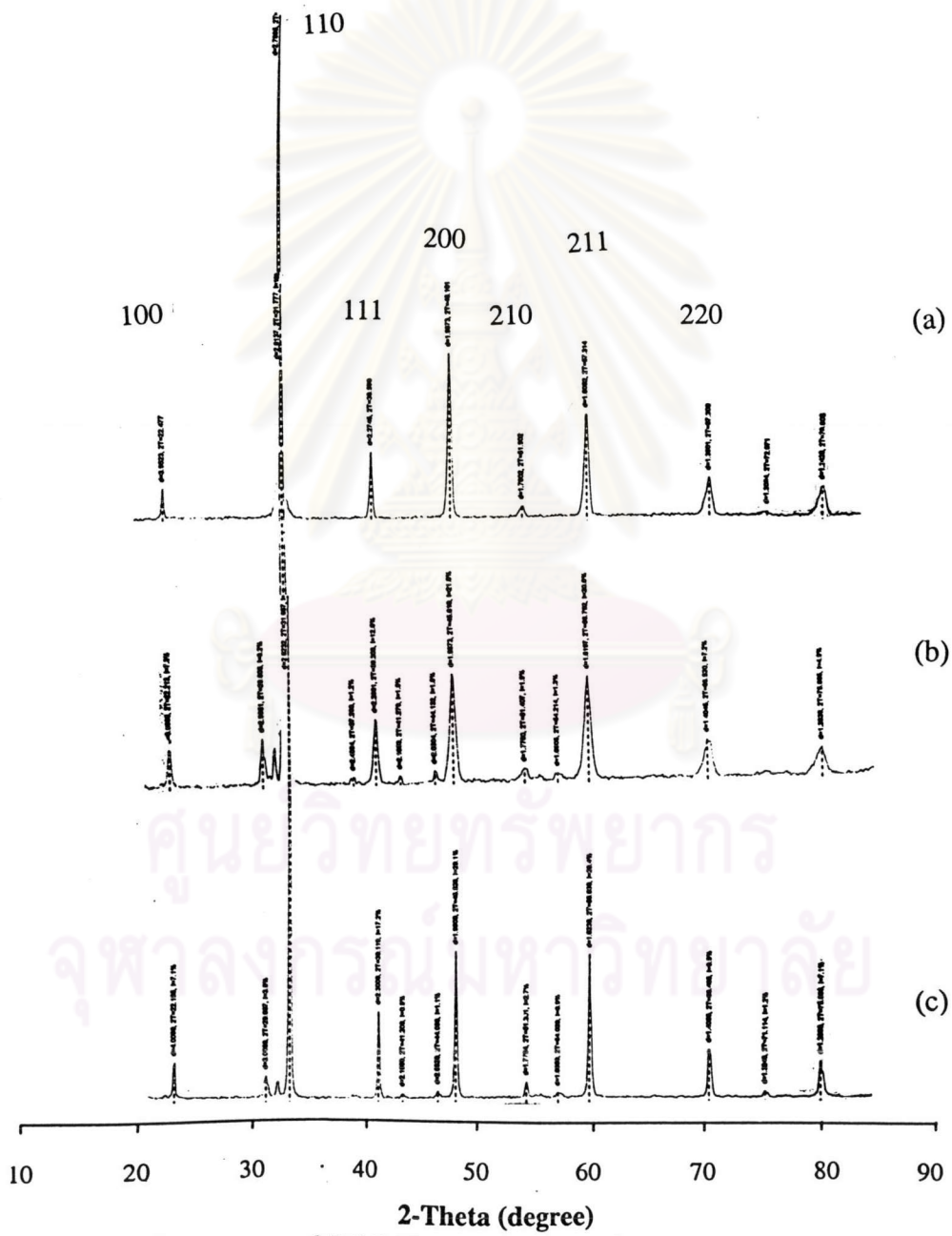

Figure 4.3 XRD patterns of BSGCF55118 (a) membrane, (b) powder synthesized by solid state method, (c) powder synthesized by modified citrate method

The XRD patterns clearly indicated that both perovskites had cubic structure regardless of the small peak at 2Θ = 30 degrees (intensity less than 4%). Surprisingly, their membranes after sintering at 1,300°C for 10 hours, had the single phase with the cubic structure as shown in Figure 4.4. It might be derived from the decomposition of the unidentified compound during sintering. Similar phenomena had been observed by Tasi et al. as well [56]. Therefore, according to the XRD pattern, the synthetic method likely had no influence on the formation of BSGCF55118 structure. However, the powder prepared by the modified citrate would have the smaller particle size due to the lower calcination temperature. This would enhance the relative density of the membrane later.

In the preliminary study, it can be concluded that the modified citrate method is suitable for the synthesis of $SrCoO_3$, $LaCoO_3$, $LaBaO_3$, and $BaFeO_3$-based perovskite. All perovskites show mainly a cubic structure. SCF had less phase purity than barium-containing perovskite and lanthanum-containing perovskite, in this order sequence. For LBCF2828 perovskite, the calcination temperature was found to affect its formation. As the calcination temperature increased, the intensity of the impurity, $BaCO_3$, decreased while La_2O_3 peak started emerging and its intensity increased with temperature. The single phase of LBCF2828 would be obtained when calcined at 1,000°C. The single-phase BSGCF55118 perovskite with the cubic structure was obtained by both using the modified citrate method with calcination at 1,000°C for 5 hours and the solid state method with the calcination of the mixture of the equal amount of BSCF5528 and BSGF5528 at 1,100°C for 5 hours.

4.3 The Influence of A-site and B-site Cation on the Formation of ABO_3-based Perovskite

With proper partial substitution of Sr in SCF1082 with Ba, Yang et al. found that a new mixed conducting material, BSCF5582 had both high oxygen permeation flux and high phase stability [51]. The results showed that the material still maintained in pure perovskite phase under the oxygen pressure from 1 atm to 10^{-5} atm at 850°C. In recent years, Ishihara et al. [10] also reported that $LaGaO_3$ has the highest oxygen ionic conductivity and the stability to reduction and oxidation [10].

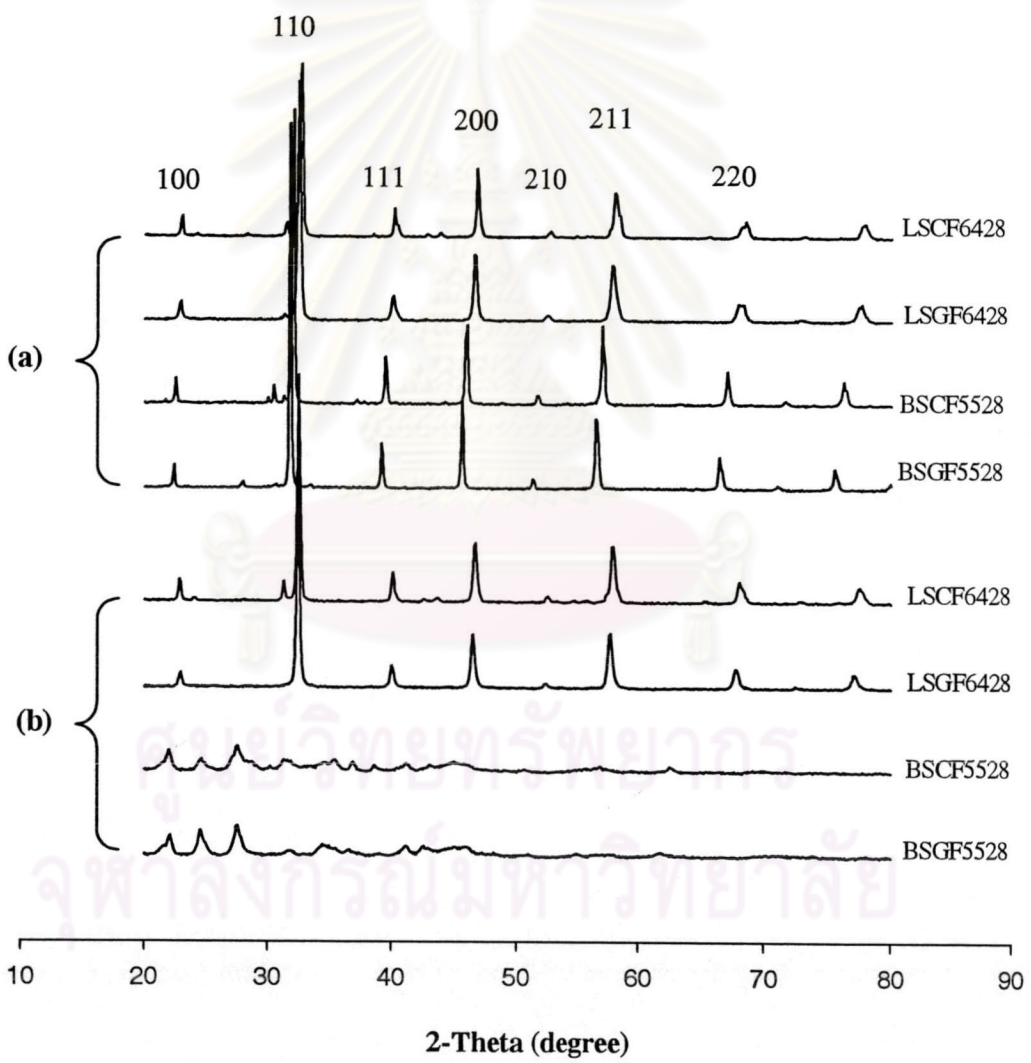

Figure 4.4 XRD patterns of LSCF6428, LSGF6428, BSCF5528, and BSGF5528 perovskites (a) before and after calcination at 1,000°C and (b) without calcination

The combination of these two studies might lead to new promissing perovskites. In particular, LSCF6428, LSGF6428, BSCF5528, and BSGF5528 perovskites were attemped to be synthesized by modified citrate method in this research work.

Figure 4.4 exhibits the XRD patterns of the four perovskites synthesized by modified citrate method before and after calcination. Several observations from these results can be drawn. The experimental conditions and data for the synthesis of these compounds were shown in Table 3.3. These XRD patterns show the single phase with the cubic structure of uncalcined lanthanum-containing perovskites, LSCF6428 and LSGF6428. The secondary phase was observed at $2\Theta = 30$ degrees of the XRD pattern of LSCF6428, but only the tiny amount appeared as the intensity was less than 5%. Both synthesized barium-containing compounds, LSCF6428 and LSGF6428, before calcination did not exhibit the perovskite characteristic peaks. In contrast, XRD patterns of both lanthanum containing perovskites, LSCF6428 and LSGF6428, before calcination indicated the existance of the perovskite structure. This might indicates that long-chain barium-citrate-nitrate probably could not be formed. This was confirmed by the observation that gel formation did not occured in the case of barium nitrate while gel clearly approved for the reactivity of lanthanun nitrate after addition of NH_4OH and before the spontaneous combustion (Table 3.3). This caused the uncalcined powder to contain the incompletely combustion compounds such as hydrocarbon, and non-perovskite structure compound. Therefore, the XRD patterns show the amorphous phase in uncalcined powder. To obtain the single-phase perovskite, the calcination of this powder was required to get rid of the remained hydrocarbon and to phase transformation. The spontaneous combustion time and weight loss were more than 20 seconds and about 20%, respectively, in the barium-containing perovskite. Comparing to lanthanum-containing perovskite, the spontaneous combustion time and weight loss were 10 second and about 2%, respectively. This indicated the high amount of hydrocarbon contained in the uncalcined powder.

It should be noted that calcination of these produced powder for both cases led to the formation of perovskites as revealed by XRD. The LSCF6428 perovskite had been formed at the stage before calcination but BSCF5528 was developed only after calcination. This conclusion was derived from the observation on the weight loss of the material before and after calcination shown in Table 4.2. Moreover, the XRD

patterns of calcined powder (in Figure 4.4) also confirmed this hypothesis. After calcination, lanthanum-containing perovskite structure did not significantly change. On the other hand, the barium-containing perovskite powder calcined at 1,000°C exhibited the single-phase perovskite with a cubic structure. Unfortunately, the influence of calcination temperature on BSCF5528 synthesized by modified citrate method was not studied. It might show the phase transformation from amorphous-uncalcined powder to single-phase perovskite as the temperature had been increased.

The unidentified phase was shown with the intensity less than 5% at $2\Theta = 30$ degree, for calcined BSCF5528. Even though the unidentified phase in both LSCF6428 and BSCF5528 perovskite structures was present at the same 2Θ, the XRD results showed the different XRD pattern of these phases, which indicated different substances. Because the trace amount of the secondary phase was present in cobalt-containing perovskite, one might infer that the modified citrate method is more suitable for the synthesis of gallium than cobalt-containing perovskite.

The lattice parameter of each perovskite was calculated from its corresponding XRD data in Table 4.2.

Table 4.2 Lattice parameter of perovskite powder

Perovskite powder	Lattice parameter (Å)	
	Before calcination	After calcination at 1,000°C
LSCF6428	3.90	3.89
LSGF6428	3.90	3.89
BSCF5528	Not available	3.96
BSGF5528	Not available	3.96

By changing the cation from La^{3+} to Ba^{2+} in A site, the lattice parameter was increased from 3.89 Å to 3.96 Å after calcination. On the other hand, changing the cation in B site from Ga^{3+} to Co^{2+} did not affect the lattice parameter. This can be attributed to the larger size of Ba^{2+}, 1.61 Å, than La^{3+}, 1.36 Å. Because of the close value of ionic radius of Ga^{3+}, 0.62 Å, and Co^{2+}, 0.65 Å, the average lattice parameters before and after metal replacement were the same.

Accordingly, it can be concluded that all compounds listed in Table 4.2 had the cubic structure. The single-phase powder was obtained from lanthanum-containing perovskite without calcination and barium-containing perovskite with calcination at 1,000°C. The lattice parameter was varied with the size of each cation.

Several other research groups [89, 90] reported the single phase of LSCF6428. Kostogloudis et al. [90] synthesized this perovskite by citrate method which the metal nitrate precursor was calcined at 1,100°C for 15 hours [90]. Teraoka et al. [89] prepared this compound by dissolving the metal nitrates or acetates into metal salts which were evaporated and calcined at 850°C for 10 hours. Comparing with the modified citrate method, the powder exhibited the single phase without calcination.

It was also reported that Yang et al. [51] prepared BSCF5582 by using a new developed method named as combined citrate and EDTA complexing method [51]. This compound was synthesized by dissolving the metal nitrates in EDTA–$NH_3.H_2O$, adding the citric acid, adjusting the pH of the solution to 6 by $NH_3.H_2O$, heating at 120–150°C for several hours, and then calcining at 950°C for 5 hours. In comparison the XRD patterns of BSCF5528 powder synthesized by the modified citrate method (Figure 4.4) with BSCF5582 prepared by Yang, it showed the same XRD patterns, which indicated that both methods were appropriative to synthesize $Ba_{1-x}Sr_x Co_{1-y}Fe_yO_{3-\delta}$. If the low calcination temperature on BSCF5528 synthesized by modified citrate method were studied, it might have shown the single-phase perovskite at the calcination temperature lower than 950°C as Yang reported.

Comparing the other synthesis method as mentions above with the modified citrate method, the single phase of lanthanum-containing and barium-containing perovskite was obtained without calcination and calcination with short time, respectively. Therefore, it could be shown that the modified citrate method was suitable for synthesis of those perovskites. Moreover, the advantages of this method included less energy consumption, simplest technology, and obtaining fine particles with a single phase.

In this experiment, the pure phase of uncalcined LSGF powder can be synthesized by the modified citrate method and, from references [53, 55], this perovskite shows the best combination of oxygen permeability and stability. Consequently, LSGF compound was chosen for this study.

4.4 Characterization of the $LaGaO_3$-Based Perovskites

In this section, the characterization of the $LaGaO_3$-based perovskites was performed by investigating the variation of Sr and Ga on the formation of these perovskites, and studying the optimum condition, i.e., pH of nitrate solution and calcination temperature.

4.4.1 The Variation of Sr Content in the $LaGaO_3$-Based Perovskite

Two series of $LaGaO_3$-based perovskites, $La_{1-x}Sr_xGa_{0.4}Fe_{0.6}O_{3-\delta}$ (x = 0.2, 0.4, and 0.6) and $La_{1-x}Sr_xGa_{0.8}Fe_{0.2}O_{3-\delta}$ (x = 0.2, 0.4, 0.5, 0.6, and 0.8), were synthesized by the modified citrate method. The calcination of these perovskites was carried out at 900°C.

4.4.1.1 Effect of Sr Content on Ga Rich $La_{1-x}Sr_xGa_{0.4}Fe_{0.6}O_{3-\delta}$

The synthesis conditions of $La_{1-x}Sr_xGa_{0.4}Fe_{0.6}O_{3-\delta}$ powders at various Sr contents both before and after calcination are shown in Table 3.4. Basically, the XRD pattern of the single-phase perovskite with a cubic structure exhibited the diffraction lines at the reflective planes 100, 110, 111, 200, 210, 211, and 220. For a $LaGaO_3$-based perovskite, these reflective lines appeared as peaks at 2θ = 22.5, 32.5, 40, 46, 52, 57.5, 67.5 degree. Therefore, all XRD patterns in Figure 4.5 clearly indicate that all synthesized compounds have the cubic structure of $LaGaO_3$-based perovskite. Because there was no other peaks presented in the XRD patterns of LSGF8246, it could be concluded that the single phase of LSGF8246 was obtained both with and without calcination.

Among the three compounds, only LSGF8246 was the single phase perovskite both before and after calcination. XRD patterns of the other two compounds, LSGF8246 and LSGF6446, both before and after calcination showed other small peaks appeared at 2θ = 24, 31, 43, 44, 56, 57, 65 degree, indicating the secondary phase in the structure. The secondary phase could be due to the existance of the oxide compounds such as, Ga_2O, La_2O, SrO, $SrGaO_7$, $SrLaGaO_4$ and La_4SrO_7 [8, 9, 79]. By comparing with the XRD patterns of the standard compounds, it could be identified as

$SrLaGaO_4$ (JCPDS-database: 24-1208). The amount of the secondary phase was slightly increased when the Sr content in $La_{1-x}Sr_xGa_{0.4}Fe_{0.6}O_{3-\delta}$ was higher than 0.2 ($x > 0.2$). However, the intensity of the highest peak ($2\theta = 31.2$) of the secondary phase did not exceed 13 % of that ($2\theta = 32.5$) of the perovskite reflection.

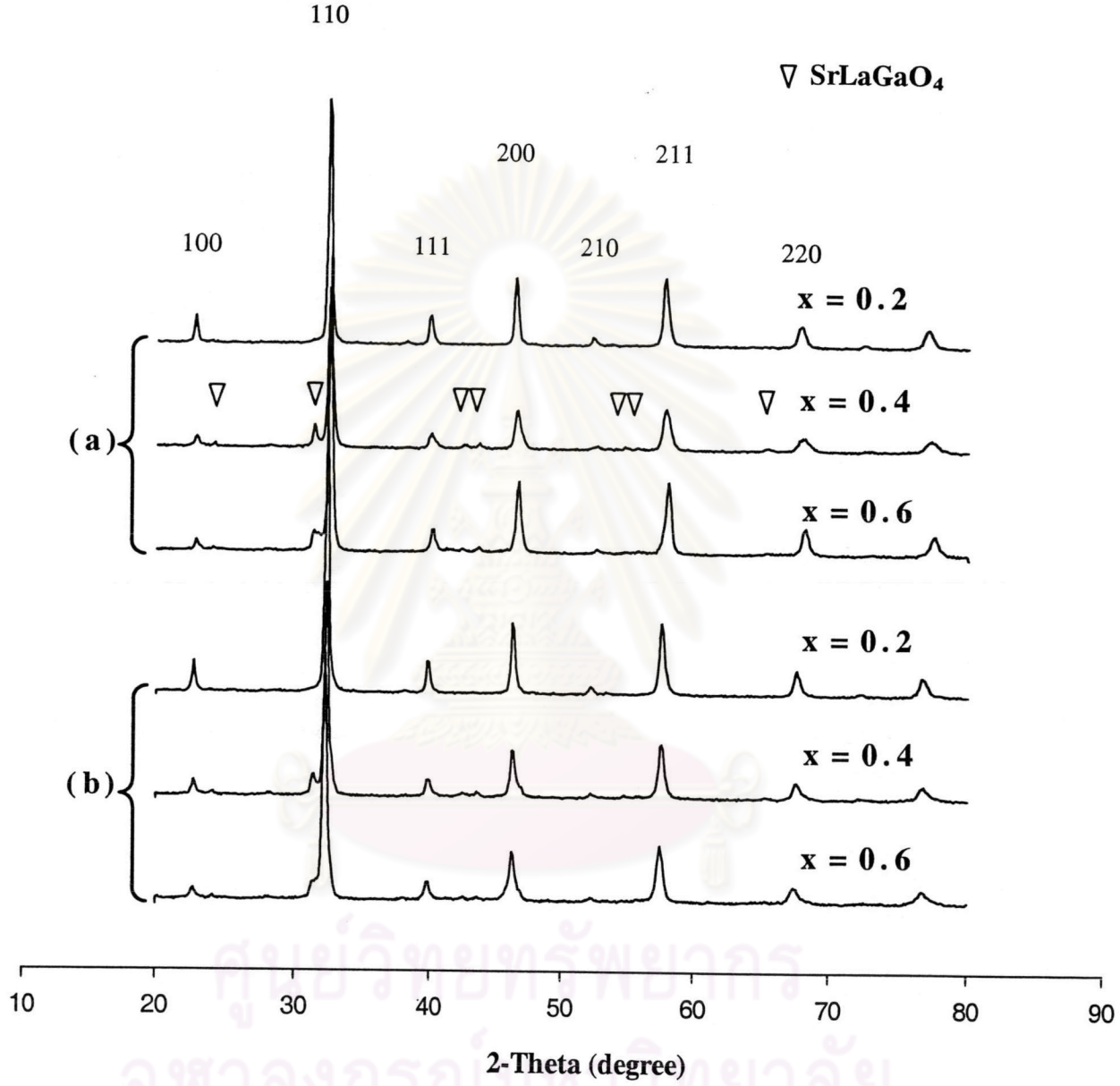

Figure 4.5 XRD patterns of $La_{1-x}Sr_xGa_{0.4}Fe_{0.6}O_{3-\delta}$ (x = 0.2, 0.4, and 0.6)
(a) calcination temperature at 900°C (b) without calcination

Since the XRD analysis of these materials indicated the formation of the perovskite-type phase with either a cubic or distorted cubic structure, and the lattice parameter of each one based on their cubic structure was calculated. Figure 4.6 shows

the plot of lattice parameter versus Sr content for both uncalcined perovskite powders and perovskite powders calcined at 900°C. In the case of the uncalcined powders, the lattice parameter was 3.91 Å for 20% Sr in the A-site and slightly increased with increasing Sr content. Generally, a larger amount of Sr doped composition will lead to the larger lattice parameter caused by the replacement of La^{3+} (ionic radius = 1.31 Å) with the larger cation, Sr^{2+} (ionic radius = 1.44 Å) [91].

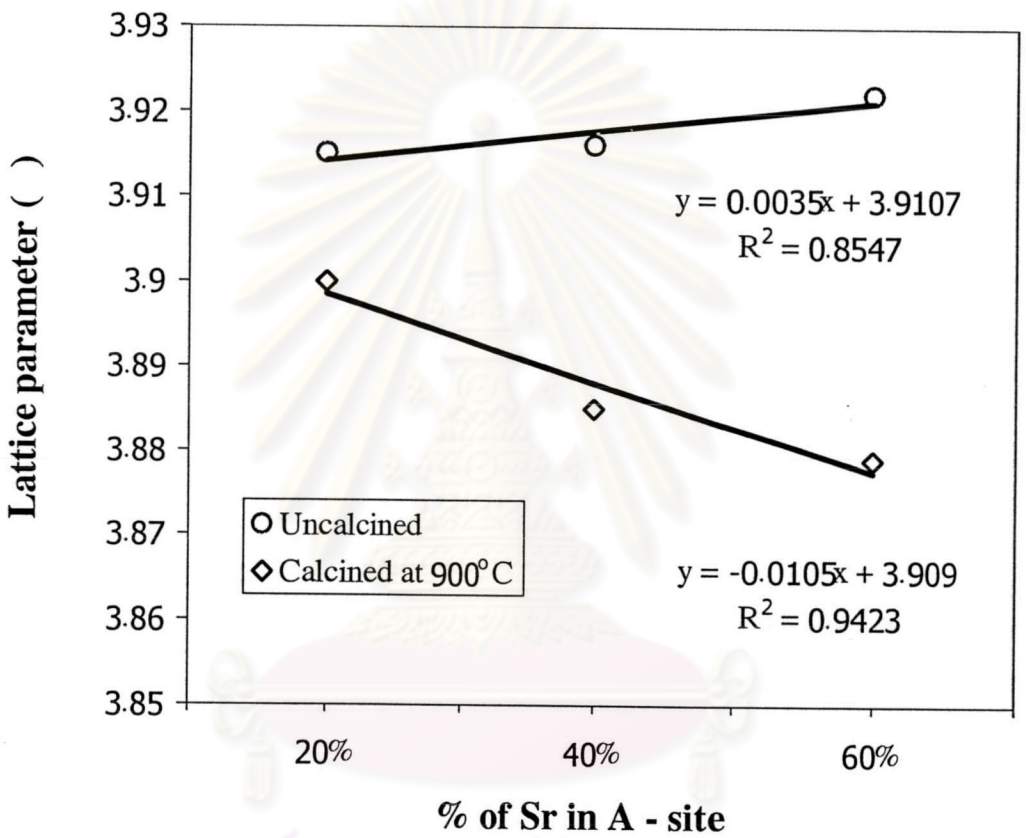

Figure 4.6 The dependence of the lattice parameter on the amount of Sr in A-site

In the case of calcination, all calcined perovskites showed smaller lattice parameters than uncalcined powders, and decreased with higher Sr content. The reason for these results is not clear yet, but the similar phenomenon was reported by Mori et al. [76] who synthesized $La_{1-x}Sr_xCrO_{3-\delta}$ (x = 0-0.3) by the solid state method.

The XRD patterns showed clearly $SrLaGaO_4$ as the secondary phase [79]. This secondary phase might be caused by the reduction of La and Sr content in the perovskite structure, which made the average lattice parameter decrease in the unit cell. Therefore, the higher Sr contents caused the appearance of higher amounts of secondary phase and lower lattice parameters. This was confirmed by the increase in

the peak intensity of the secondary phase in LSGF6446 and LSGF4646 from less than 4% of uncalcined powders to 10.8% and 12.7% of calcined powders, respectively.

4.4.1.2 Effect of Sr Content on Ga Lean $La_{1-x}Sr_xGa_{0.2}Fe_{0.8}O_{3-\delta}$

Ming et al. [13] reported that the perovskite LSGF5528 had a higher oxygen permeation flux than the non-perovskite oxide SFC. They also observed that Sr content increased the mixed ionic and electronic property. Therefore the variation of Sr content in $La_{1-x}Sr_xGa_{0.2}Fe_{0.8}O_{3-\delta}$ was studied in this research.

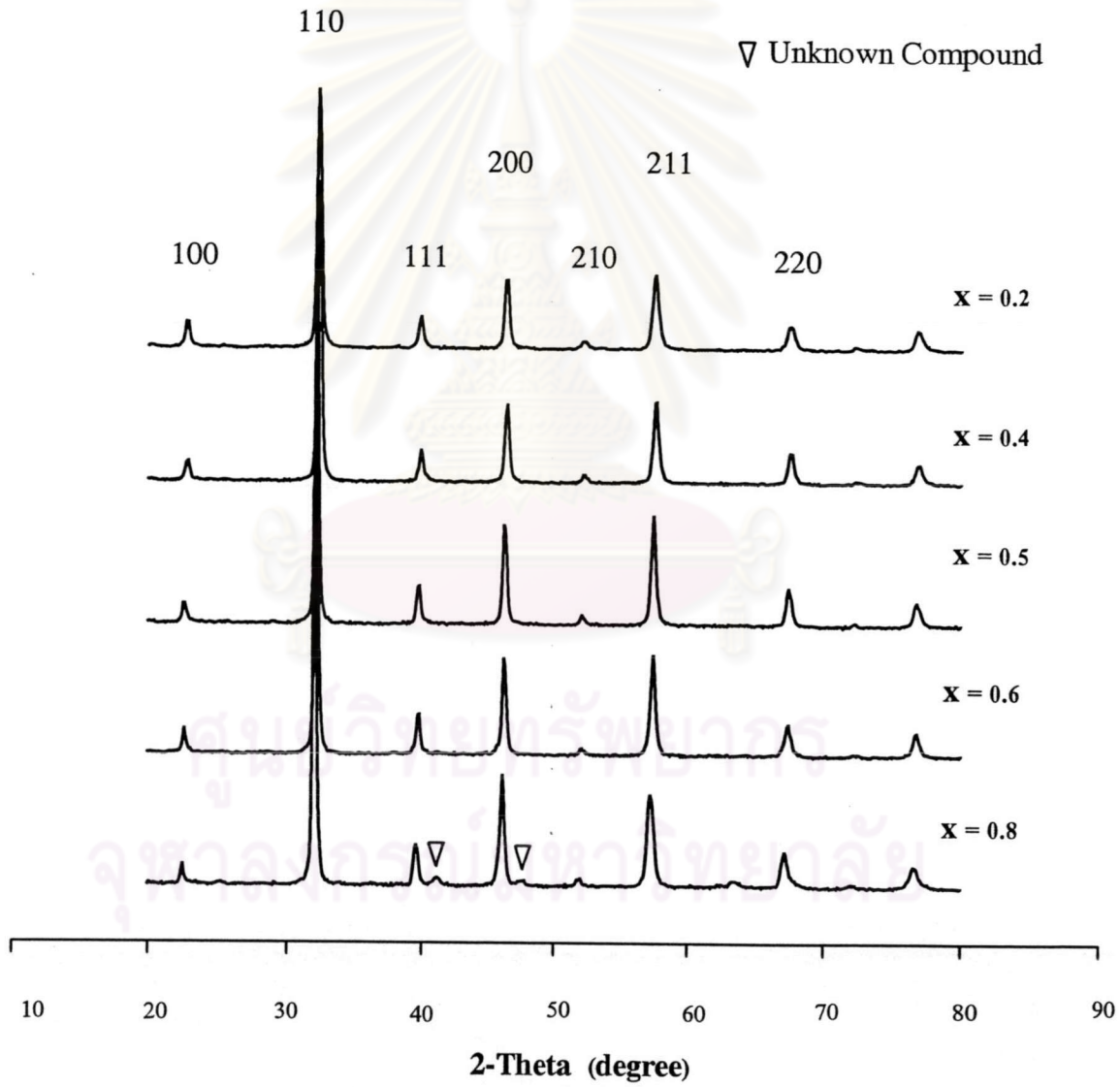

Figure 4.7 XRD patterns of uncalcined $La_{1-x}Sr_xGa_{0.2}Fe_{0.8}O_{3-\delta}$ (x = 0.2, 0.4, 0.5, 0.6, and 0.8)

The list of synthesis conditions and the XRD patterns of all uncalcined $La_{1-x}Sr_xGa_{0.2}Fe_{0.8}O_{3-\delta}$ was shown in Table 3.5 and Figure 4.7, respectively. A pure perovskite phase with a cubic structure could be observed in all compositions except for x = 0.8 where the unknown peaks existed (2θ = 42 and 48). Because only two unknown peaks were observed, these could not be identified by XRD. However, these peaks might be belonged to the compound of Sr due to the observation of peak at the highest amount of Sr (x = 0.8). The intensity of the highest peak of the secondary phase did not exceed 5 % of that (2θ = 32.5) of the perovskite reflection. Because the intensity of the secondary phase in LSGF4628 (< 5%) was less than that in LSGF4646 (<13%), therefore, the single-phase perovskites seemed to be obtained from the high Sr-content in Ga lean more than Ga rich perovskite.

A homogeneous LSGF5528 synthesized by self-propagating high-temperature synthesis (SHS) was also reported by Ming et al. [13]. By the XRD analysis, the LSGF5528 synthesized by the modified citrate method showed the single-phase structure as well as synthesized by SHS. However, SHS method involved several steps, i.e. mixing metal oxides, pressing into pellet, pre-heating at 1,400°C, milling into powder, making membrane, and sintering at 1,380°C. Therefore, the modified citrate method is more convenient for synthesizing $La_{1-x}Sr_xGa_{0.2}Fe_{0.8}O_{3-\delta}$ due to the less energy consumption and simple technology.

Since the perovskite oxide, $La_{0.5}Sr_{0.5}Ga_{0.2}Fe_{0.8}O_{3-\delta}$ or LSGF5528, synthesized by SHS had been proved to be suitable for use as a membrane in syngas production, it remained the cubic structure from 20 to 860°C in a reducing environment with an oxygen partial pressure of about 10^{-17} atm. Furthermore, it was reported that it gave a higher oxygen permeation flux than the non-perovskite oxide SCF in the application at the CH_4 partial oxidation temperature. Therefore $La_{1-x}Sr_xGa_{0.2}Fe_{0.8}O_{3-\delta}$ synthesized by the modified citrate method was expected to be a good membrane in syngas production.

4.4.2 The Variation of Fe Content in $LaGaO_3$-Based Perovskite

For providing the high oxygen flux in methane conversion, a large amount of Sr is required, as it would increase the electronic and ionic conductivity. It has also been reported that the suitable Sr content was in the range of x = 0.2-0.4 [89]. Besides doping with Sr at A-site, it was reported that doping with Fe at B-site also increased the high oxygen flux in $La_{0.8}Sr_{0.2}Ga_{1-y}Fe_yO_{3-\delta}$ series where y = 0.2-0.5 and the appropiate amount of doped Fe was in the range of y = 0.3-0.4. The single phase of these series were synthesized by solid state method, which the metal oxides was calcined at 1,000-1,100°C for 6-10 hours [9, 10].

Therefore $La_{0.6}Sr_{0.4}Ga_{1-y}Fe_yO_{3-\delta}$ with the amount of 40% Sr was chosen to obtain the single phase by varying the amount of Fe. Moreover, since the synthesis of $La_{0.4}Sr_{0.6}Ga_{1-y}Fe_yO_{3-\delta}$ series has not been reported in both solid state method and modified citrate method, these series also were chosen to study the effect of Fe on the formation of $LaGaO_3$-based perovskite.

$La_{0.6}Sr_{0.4}Ga_{1-y}Fe_yO_{3-\delta}$ (y = 0.2, 0.4, 0.5, 0.6, and 0.8) and $La_{0.4}Sr_{0.6}Ga_{1-y}Fe_yO_{3-\delta}$ (y = 0.4, 0.6, and 0.8) were all synthesized from the basic solution and then calcined at 900°C. The lists of the synthesis conditions of both perovskite series were shown in Table 3.6 and Table 3.7. Phase formation for all compounds with and without calcination was determined by the X-ray diffraction. For $La_{0.6}Sr_{0.4}Ga_{1-y}Fe_yO_{3-\delta}$ series, it was found that when the amount of Fe increased from x = 0.6 to 0.8, a single phase of LSGF6428 was obtained. On the other hand, the secondary phase of $SrLaGaO_4$ dramatically increased with decreasing Fe content in both with and without calcination, as shown in Figure 4.8. Even though the diffraction peaks assigned to the secondary phases were observed, the typical XRD patterns of $LaGaO_3$ based structure were exhibited for all powders. From Table 3.6, the lanthanum-containing precursor precipitated at pH = 4. The spontaneous combustion time was about 10 second and the weight loss after calcination was less than 3%. These indicated that there was sufficient fuel to decompose the citrate salt to carbon dioxide and water.

Comparing with the solid state method done by Ishihara et al. [10] who synthesized the single phase $La_{0.8}Sr_{0.2}Ga_{1-y}Fe_yO_{3-\delta}$ where y = 0.2-0.5, the modified citrate method seems to be suitable for synthesizing the single phase LSGF6428, which has the higher Fe content than the previous once. The single-phase LSGF

perovskite with high Ga content could not be synthesized by wet chemical method, therefore, it might be possible that, for achieving the single phase of the Ga rich perovskties, the temperature higher than the flame temperature to transform the gel phase to solid phase is required.

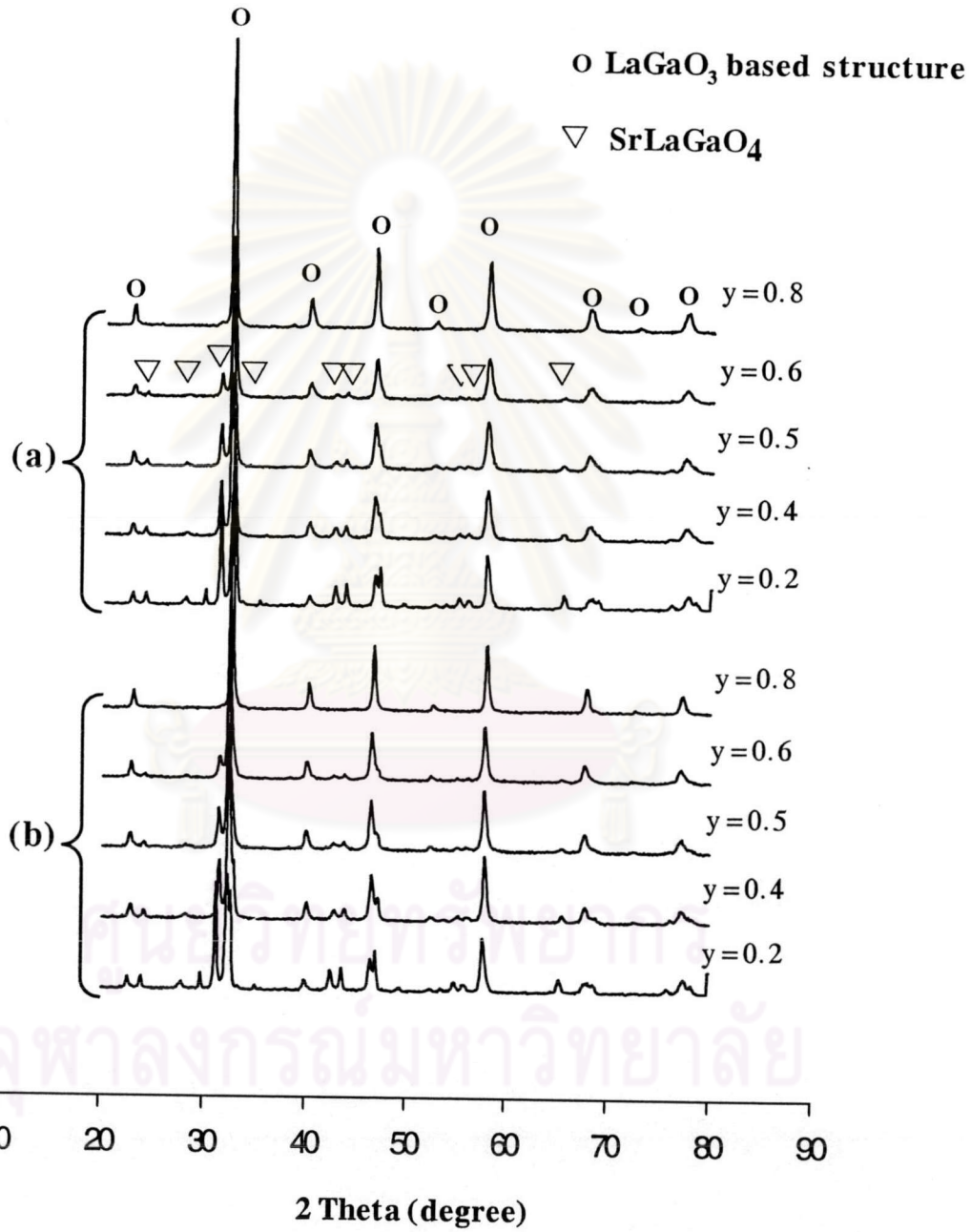

Figure 4.8 XRD patterns of $La_{0.6}Sr_{0.4}Ga_{1-y}Fe_yO_{3-\delta}$ (y = 0.2, 0.4, 0.5, 0.6, and 0.8) (a) calcination at 900°C and (b) without calcination.

For $La_{0.4}Sr_{0.6}Ga_{1-y}Fe_yO_{3-\delta}$ series, these perovskites exhibited the similar phenomenon as $La_{0.6}Sr_{0.4}Ga_{1-y}Fe_yO_{3-\delta}$ series, leading to the single phase of LSGF4628. The XRD patterns of uncalcined perovskites are shown in Figure 4.9.

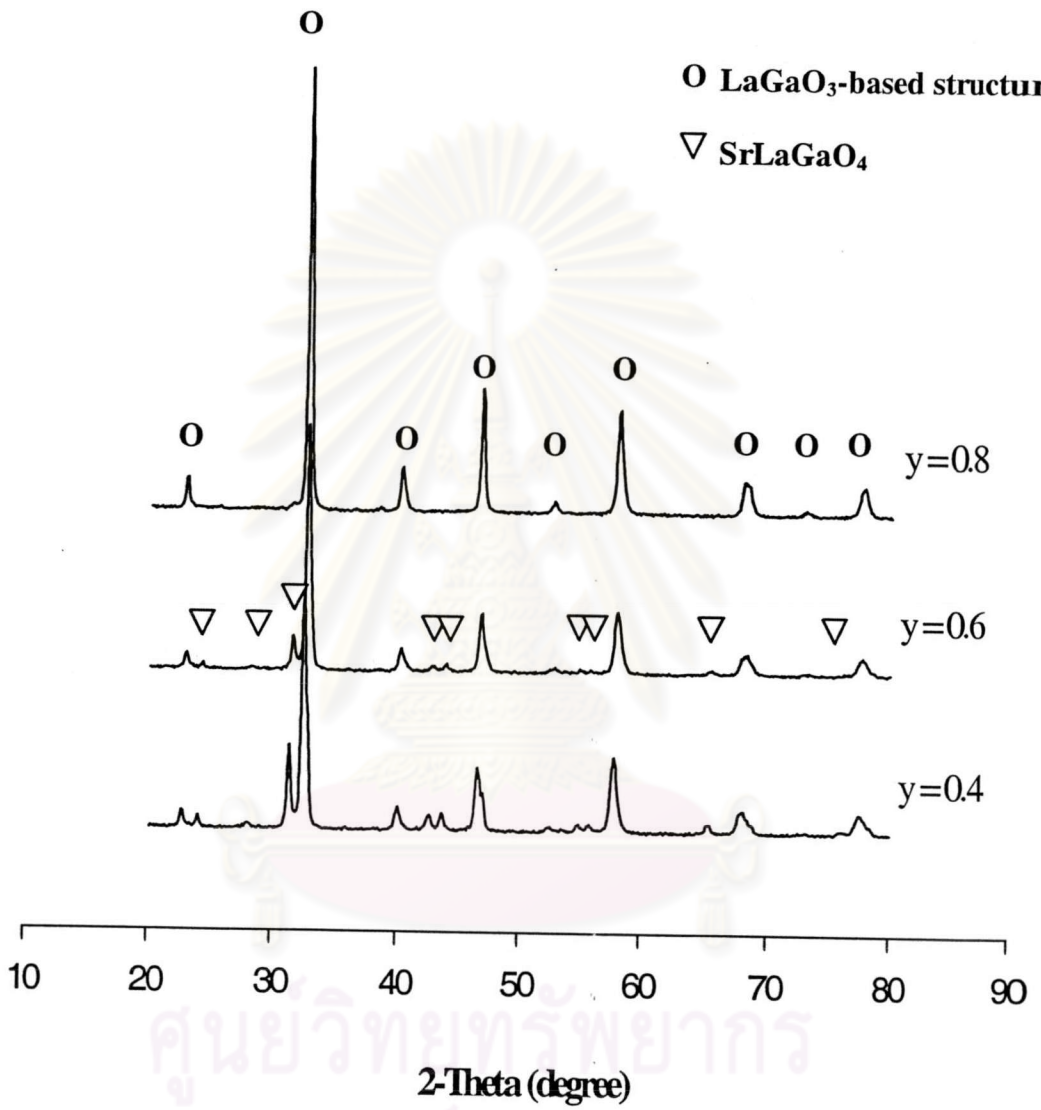

Figure 4.9 XRD patterns of uncalcined $La_{0.4}Sr_{0.6}Ga_{1-y}Fe_yO_{3-\delta}$ (y = 0.4, 0.6, and 0.8)

4.4.3 The Effect of Sr and Fe on the Formation of $LaGaO_3$-based Perovskite

For varying the four series of Sr and Fe doped $LaGaO_3$-based perovskite, the effect of doped metals on the formation of $LaGaO_3$ was concluded by means of XRD analysis as in Table 4.3.

Table 4.3 Secondary phases found in differently doped LSGF perovskites

LSGF Composition	Observed Secondary Phase
8228	No
6428	No
5528	No
4628	No
2828	Traces of unknown compound
8246	No
6446	Traces of $SrLaGaO_4$
4646	Traces of $SrLaGaO_4$
6455	$SrLaGaO_4$
6464	$SrLaGaO_4$
6482	$SrLaGaO_4$
4664	$SrLaGaO_4$

In this work, $LaGaO_3$-based perovskite was divided into 2 main groups, Ga-lean perovskite (y = 0.8) and Ga-rich perovskite (y = 0.4 and 0.6). The analysis shows that the concentration of Sr and Fe in the matrix of LSGF powders corresponds to $x = 0.2$ for $y < 0.8$ and $x = 0.6$ for $y = 0.8$. This means that the solubility limit of each dopant depends on the concentration of the other dissolved in $LaGaO_3$. The samples with $x \leq 0.2$ and $x \leq 0.6$ for Ga rich and Ga lean, respectively, belong to single-phase $LaGaO_3$-based perovskite. If excess Sr was added, $SrLaGaO_4$ secondary phase was clearly formed in addition to the Ga-rich perovskite, while, the Ga-lean perovskite shows the other unknown secondary phase when $x > 0.6$. It might be because, for the less amount of Ga, there was not enough Ga to form the complex of

$SrLaGaO_4$ secondary phase. On the other hand, this unknown compound would be the complex of Sr and Fe due to the high amount of these metals.

The modified citrate method seems to be suitable for synthesizing the single phase Ga-lean or high Fe-content perovskite. The results showed the single phase with the cubic structure was obtained from LSGF8228, LSGF6428, LSGF5528, LSGF4628, and, LSGF8264 both with and without calcination. Considering only the variation of Fe in all compositions except at x = 0.2, the secondary phase was clearly observed when the amount of Fe was decreased from x = 0.8 to 0.6 and 0.4, while the variation of Sr scarcely enhanced the secondary phase. Besides the influence of composition, the synthetic conditions such as, the amount of citric acid, pH of nitrate solution, and calcination temperature, should influence on the formation of LSGF powders. Therefore the impurity phase of Ga-rich LSGF6482 and the pure phase of Ga-lean LSGF6428 were chosen for further study on the optimum condition of the pH of the nitrate solution and calcination temperature.

4.4.4 The Variation of pH of Nitrate Solution

The high value of pH was expected to enhance the formation of the single phase perovskite and its physical appearances such as small particle size, better crystal structure since combustion was more rapid and complete at higher temperatrues. This was due to the high pH generating the high amount of NH_4NO_3, which served as a fuel for spontaneous combustion and caused the high flame temperature. This phenomenon was comfimed by Chick et al. [64], who synthesized $La(Sr)CrO_3$ and $La(Sr)MnO_3$ by the glycine-nitrate combustion method. The glycine used, instead of citric, performed two functions. First, it formed complexes with metal cations and increased their solubility. Second, the glycine served as a fuel during charing. It was reported that the optimum properties were obtained when the glycine/nitrate ratio was adjusted to yield the peak flame temperature. This phenomenon was also supported by Suresh et al. [66], who synthesized $La_{1-x}Sr_xFeO_{3-\delta}$ by using the solution combustion method of corresponding metal nitrates, oxalyl dihydrazide (ODH) or tetra formal tris azine (TFTA). The mark difference in the optimum properties, phase purification and particle size, of $La_{1-x}Sr_xFeO_{3-\delta}$ prepared by ODH and TFTA mixtures depended on the nature of the fuel which controls the nature of combustion (smouldering and flaming). Therefore, LSF perovskite prepared by TFTA has the good optimum properties because the combustion is flaming with TFTA.

Even though, from the previous section, LSGF6482 and LSGF6428 powder had been synthesized at high pH (about 9), the various pH of nitrate solution from 1-9 of both compositions was studied. For non-single phase of LSGF6482, it was expected to show the developing of phase transformation, while, for single phase of LSGF6428, the optimum condition could be obtained. The metal-citrate complex solution was titrated with NH_4OH until the desired pH was reached. The pH of the solution was adjusted corresponding to the change of solution color or solution phase. The powder was ground by using a mortar and a pestle before and after calcination at 900°C for 5 hours. The lists of synthesis conditions for LSGF6482 and LSGF6428 were shown in Table 3.8 and Table 3.9, respectively.

4.4.4.1 Ga Rich in $La_{0.6}Sr_{0.4}Ga_{0.8}Fe_{0.2}O_{3-\delta}$

Figure 4.10 showed the XRD patterns of uncalcined LSGF6482 at different pH. It was certainly clear that the uncalcined powder showed perovskite characteristic peaks, which indicated that some perovskite structure particles existed in the uncalcined powder. The secondary phase of $SrLaGaO_4$ was observed in all range of pH. The XRD pattern of perovskite synthesized at all ranges of pH was scarely changed, indicating that high pH did not enhance the single phase of Ga rich perovskite. At pH = 0.80, the intensity of unknown compound

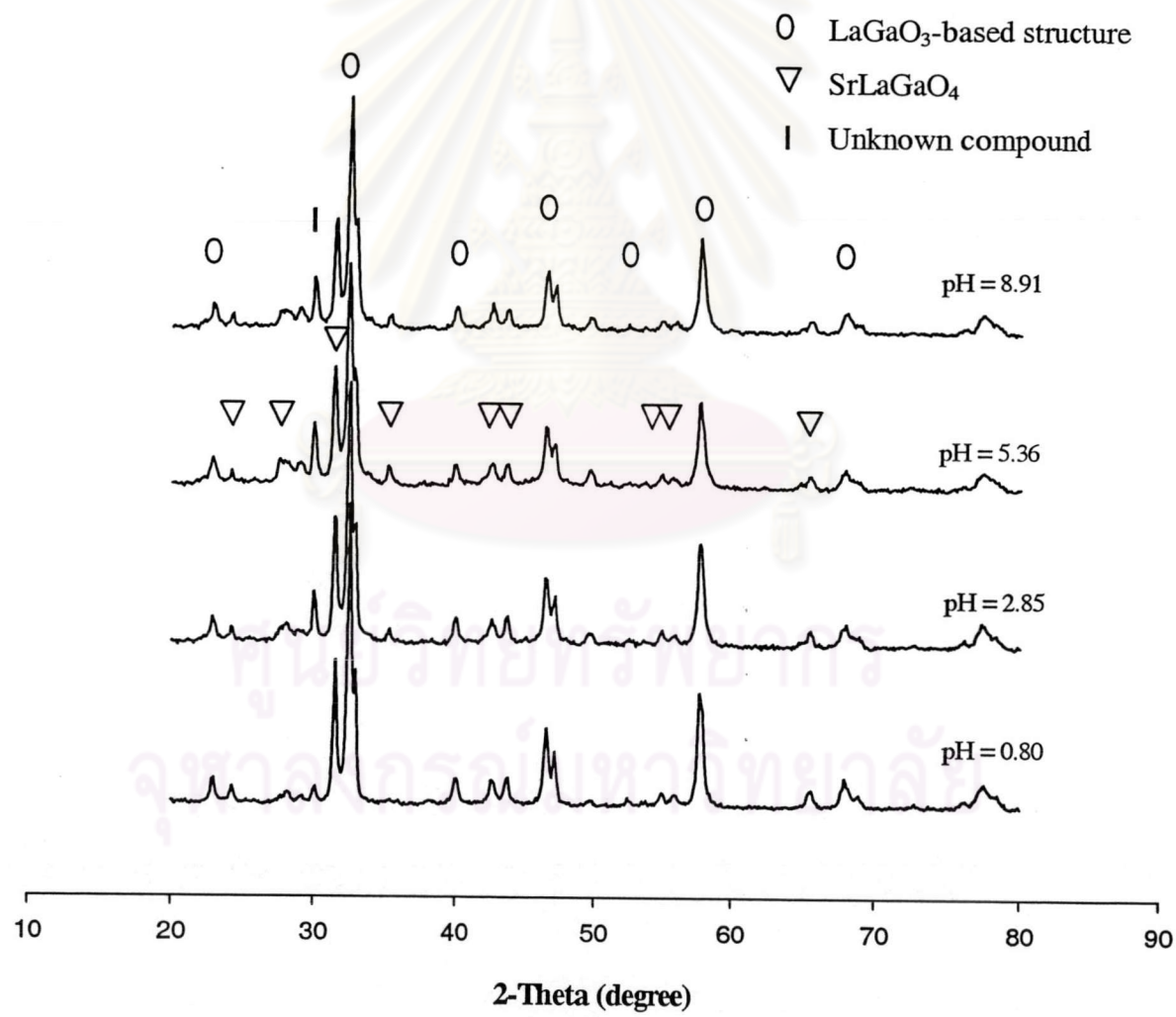

Figure 4.10 XRD patterns of uncalcined LSGF6482 at different pH.

existed at $2\Theta = 30$ degrees seemed higher than that from the higher pH. The reason for this phenomenon has not been found yet, therefore it should be further studied.

After calcination at 1,300°C, the XRD analysis showed the same XRD pattern as uncalcined powder. Therefore the XRD patterns of calcined powder were not shown here. The result shows that the phase purity of LSGF6482 could not be formed neither by pH nor by calcination. It might be because the E_a for the crystalline phase of Ga rich-containing perovskite was so high that the temperature of spontaneous flame could not reach the single phase as discussed in section 4.4.2. Therefore, some LSGF and other metal complex compounds were presented as seen form a lot of peaks in Figure 4.10. The similar XRD patterns of uncalcined and calcined powder might be an indication that during the spontaneous combustion all compounds in the powder formed the stable lattice, separating with each other. The result was that even calcination at high temperatures, the metal complex oxides would not combine with each other and then reconstruct to the single-phase perovskite.

4.4.4.2 Ga Lean in $La_{0.6}Sr_{0.4}Ga_{0.2}Fe_{0.8}O_{3-\delta}$

Figure 4.11 shows the XRD patterns of the LSGF6428 samples. The results show that a single-phase $LaGaO_3$ perovskite was obtained in all powder except pH = 1.10. It should be noted that all solutions were clear except at pH = 3.39. At this pH, the precipitation might be due to the polymerization of metal citrate-nitrate complex, which occurred and did not disappear during the combustion process. However, the obtained powder still was the single phase, which was the same as the others. This might be due to the fact that, with the sufficient NH_4NO_3, this powder could crystallize at the spontaneous combustion temperature. The powder after the spontaneous combustion was then ground by using a mortar and a pestle both before and after calcination at 900°C for 5 hours.

XRD patterns of LSGF6428 at pH = 1.10 showed that the secondary phase of $SrLaGaO_4$ existed in both the uncalcined powder and the powder calcined at 900°C. It was possible that at pH = 1.10 the amount of the NH_4NO_3 for initiating the combustion was not sufficient to develop the high flame temperature. Generally, the combustion involved two components, fuel and oxidant (normally air) which were heated to the

suitable circumstance [92]. If there was sufficient amount of fuel, the combustion tended to give the high rate of flame propagation leading to the high temperature of the flame and less combustion time. Therefore, at pH = 1.10, the spontaneous combustion might have taken place at a low rate, resulting in the longer spontaneous combustion.

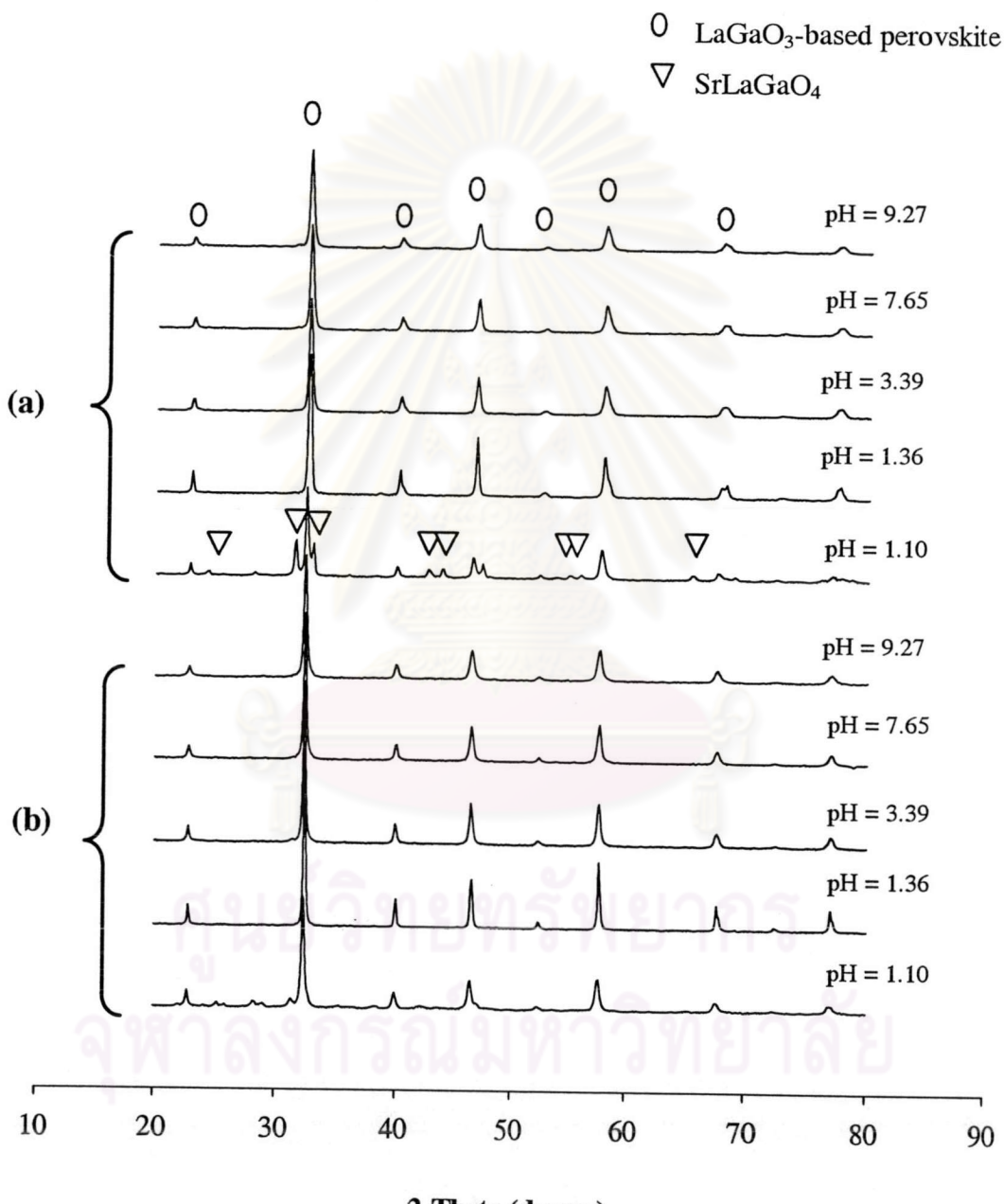

Figure 4.11 XRD patterns of LSGF6428 at different pH

(a) calcination at 900°C and (b)without calcination.

This is substantiated by the fact that the spontaneous combustion time for the synthesized LSGF6428 at pH = 1.10 was about 20 sec, longer than those of higher pH compositions (about 10 sec). The XRD data also provided the measurement of the lattice parameters for the uncalcined and calcined powder of 3.90 and 3.88 Å, respectively.

One of the important factors for the formation of a membrane disc is the particle size distribution of calcined powder. The particle size distributions of calcined powder are shown in Figure 4.12. The results obtained from a centrifugal particle size analyzer showed a significant difference between powder synthesized from pH in the range of 3.39-9.27 and the powder synthesized from pH = 1.36. The average particle size was 0.57 μm for the pH in the range of 3.39-9.27 while it was 1.70 μm for pH=1.36.

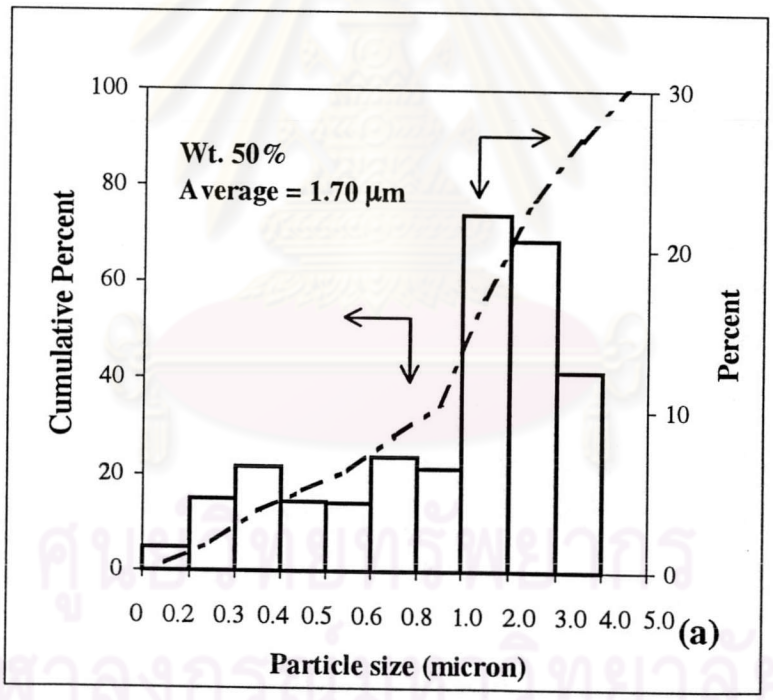

Figure 4.12 Particle size distribution of calcined LSGF6428 at different pH: (a) pH = 1.36, (b) pH = 3.39, (c) pH = 7.65, (d) pH = 9.27.

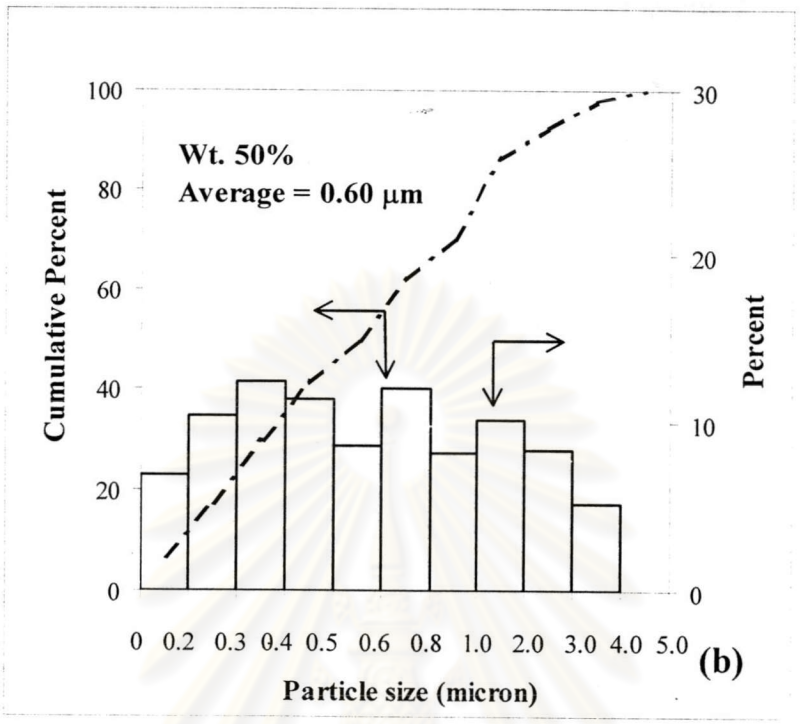

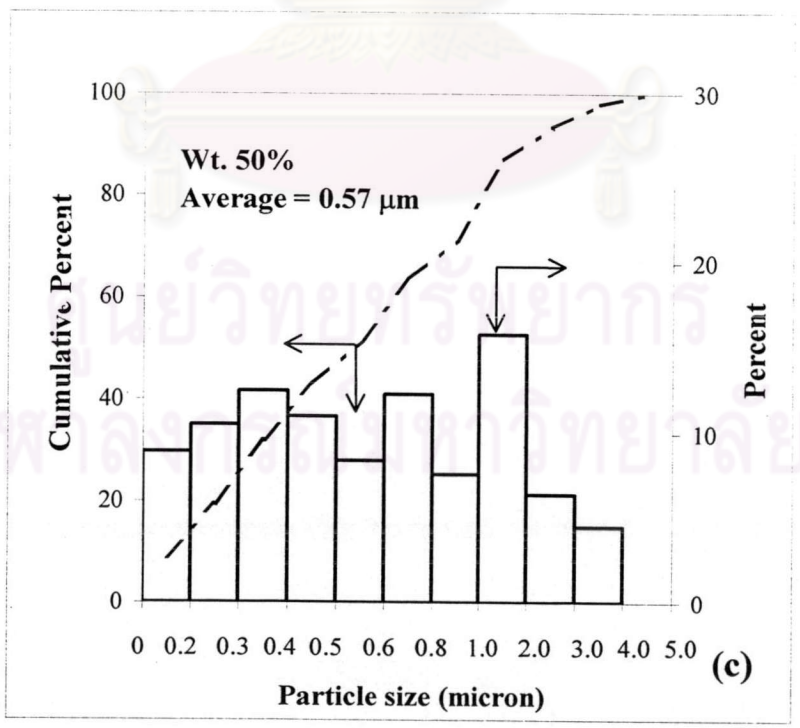

Figure 4.12 (Continued)

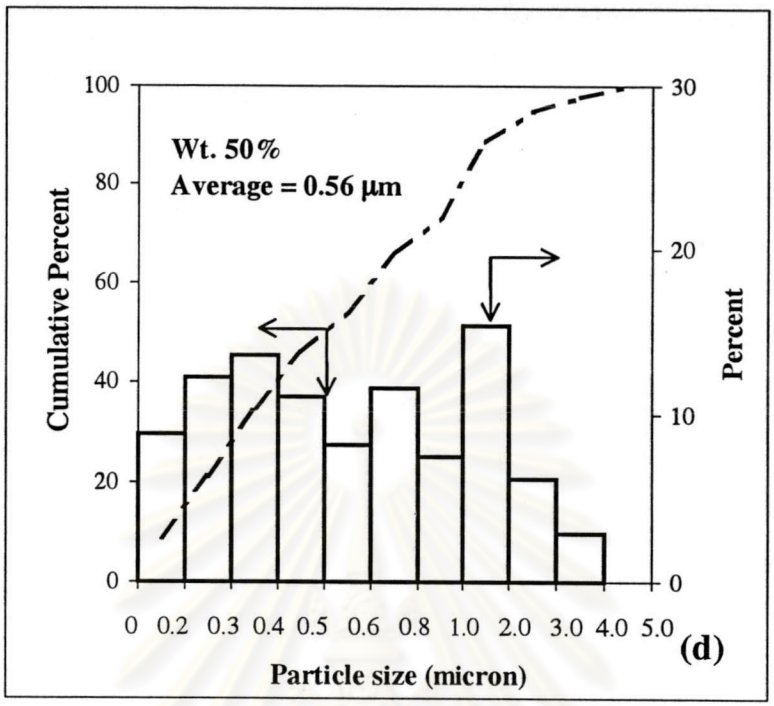

Figure 4.12 (Continued)

The SEM pictures of the calcined LSGF6428 powder synthesized at pH = 9.27 are shown in Figure 4.13. They indicate that the particle size is about 0.6 μm. The particle sizes of other powder are similar to LSGF6428, though SEM pictures are not shown here. Comparing between Figures 4.12 and 4.13, it can be seen that powder calcined and ground by mortar include agglomerated powder.

The marked difference in the particle size of LSGF6428 prepared at pH = 1.36 and pH in the range of 3.39-9.27 can be attributed to the concentration of the metal citrate-nitrate solutions. In the case of the impregnation of the metal salt solutions to the pores of the support (e.g the impregnation of $FeCl_3$ solution in the zeolite), the average size of the metal particles depends on the concentration of the solutions. The high metal concentrations tend to give larger particles than the lower ones [93]. According to this hypothesis, the perovskite obtained at pH = 1.36 should consist of the largest particle size since at pH = 1.36, the concentration of the solution was approximately 20% higher than the solution at pH = 9.37.

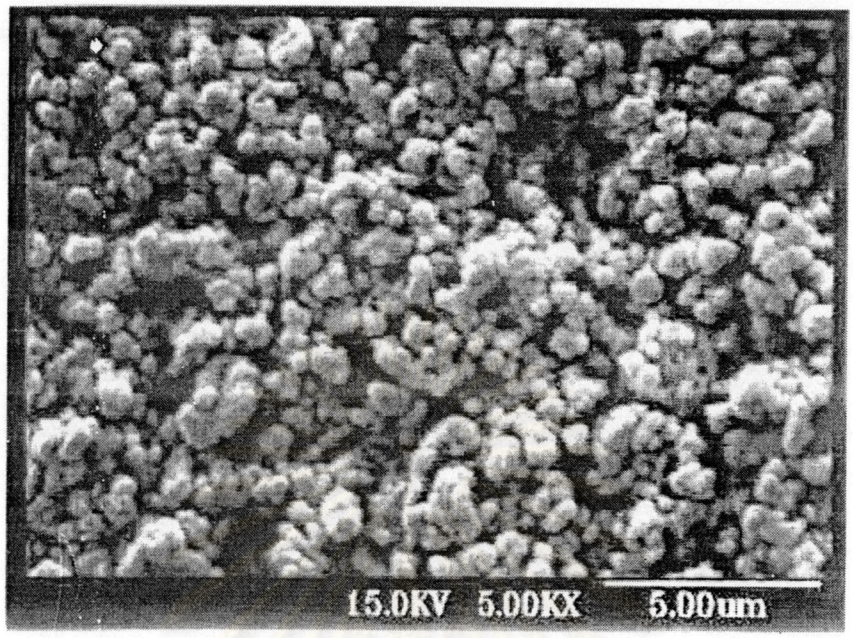

(a)

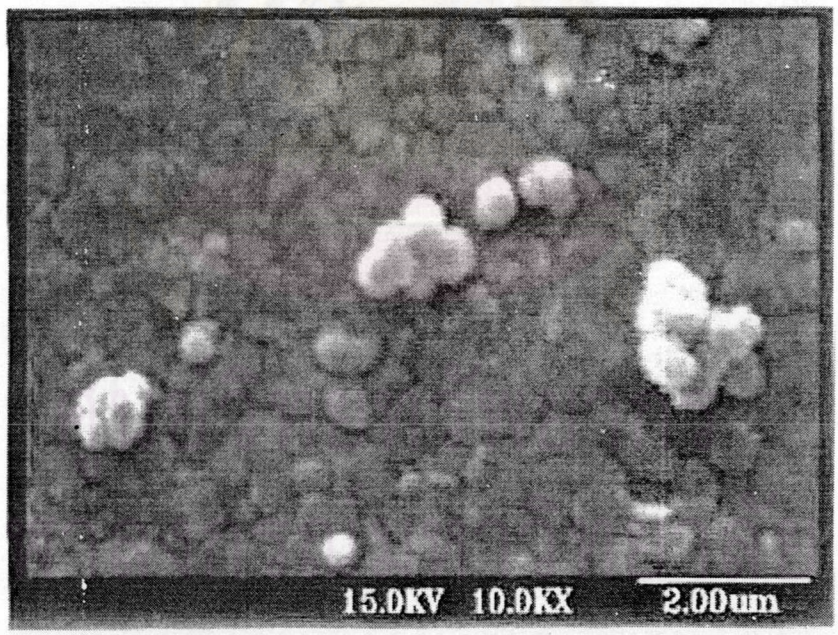

(b)

Figure 4.13 SEM pictures of calcined powder LSGF6428 synthesized pH =9.27 (a) cluster, (b) single.

Considering the influence of pH of the nitrate solution in the range of 1-9 on the formation of LSGF perovskite, it can be concluded that pH of the nitrate solution did not enhance the phase purification of LSGF6428. A single phase of LSGF6428 was obtained in all pH except pH = 1.10. In stead of phase purity, the pH influences the particle size of perovskite powder. The average particle size of LSGF6428 decreased with the increase of pH. It was approximately 1.70 and 0.57 μm at pH=1.36 and pH in the range of 3.39-9.27, respectively. Accordingly, pH = 3.39 was the optimum pH for the synthesis of the single-phase LSGF perovskite with the fine particle.

Even though the calcination temperature did not enhance the phase purity of Ga rich perovskite (LSGF6482), for the lower Ga content perovskite, the calcination temperature might influence the phase purity. Therefore, the calcination temperature should be further studied.

4.4.5 The Influence of Calcination Temperature on Phase Purification

For the comparison of calcination temperatures, the same uncalcined powder was used as the starting material for each experiment. For the determination of the influence of the calcination temperatures, non- single phase of LSGF6446 and single phase of LSGF6428 powder was calcined at temperature in the range of 800-1,400°C for 5 hours. The list of synthesis conditions for LSGF6446 and LSGF6428 were shown in Table 3.10 and 3.11, respectively.

4.4.5.1 Non-Single Phase of Ga Rich in $La_{0.6}Sr_{0.4}Ga_{0.4}Fe_{0.6}O_{3-\delta}$

The single phase of Sr and Fe-doped $LaGaO_3$-based perovskite was synthesized by the conventional method which the metal oxides were calcined at 1,000-1,100°C for 6-12 hours [10, 12, 94]. Therefore, the phase purity of non-single phase LSGF6446 was expected to improve as a function of calcination temperature especially at 1,000°C. The XRD patterns of LSGF6446 uncalcined powder and calcined at 900-1000°C are shown in Figure 4.14.

The XRD analysis of this work indicated that the intensity of the highest peak ($2\theta \approx 31$) of $SrLaGaO_4$ secondary phase did not disappear with increasing of calcination temperature. On the other hand, this intensity increased with increasing temperature. Therefore, it was clearly shown that the single phase of LSGF6446 was not obtained as LBCF and barium-based perovskite when the calcination temperatures were increased. By the modified citrate method, the single-phase perovskite was not obtained when calcined at 1,000°C for 5 hours as by the conventional method. It might be because the Ga contained in the citrate-nitrate precursor, whose Ga content was more than 20%, required the high temperature of spontaneous combustion to transform to single-phase of LSGF perovskite. This similar phenomenon was observed by Chick et al [64] who synthesized $LaSrMnO_3$ by glycine-nitrate combustion method. They found that, under moderately fuel-rich condition, $Sr(NO_3)_3$ was detected in the ash. Accordingly, the calcination temperature could not promote the solid state reaction between the perovsktie phase and secondary phase while the single phase would be obtained in the conventional

method. Moreover, the presence of the secondary phase might be resulted from the use of high amount of citric acid, twice as much as the metal cations, in all cases. This would promote the secondary phase from the complex of Sr and Ga with citric acid. As reported by Baythoun et al. [62], if the high amount of citric acid was used, the secondary phase of Mn_2O_3 was presented from the complex of Mn and citric acid as in Equation (10). Therefore the amount of citric acid should be further studied.

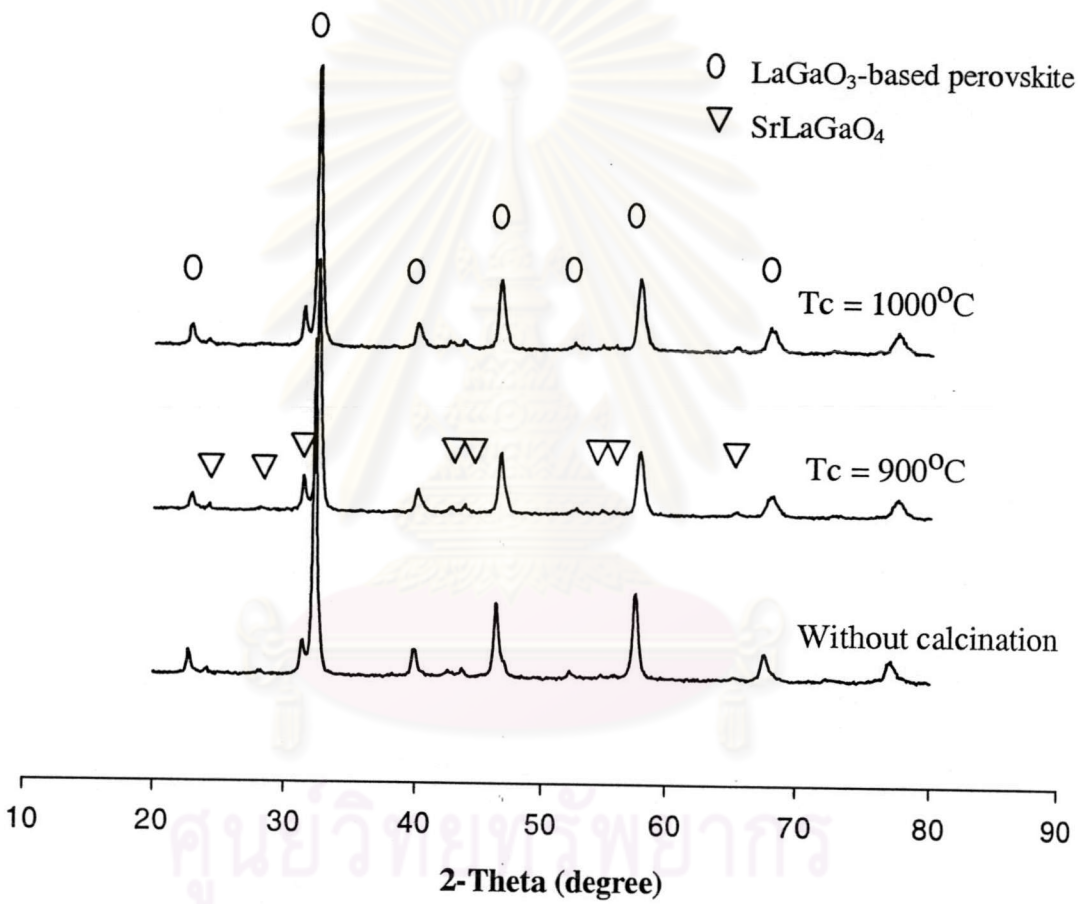

Figure 4.14 XRD patterns of LSGF6446 without calcination and after calcination

4.4.5.2 Single Phase of Ga Lean in $La_{0.6}Sr_{0.4}Ga_{0.2}Fe_{0.8}O_{3-\delta}$

The characteristic XRD patterns of the LSGF6428 without calcination and after calcination are shown in Figure 4.15. Lattice parameters are shown in Figure 4.16. The weight loss of powder after calcination as a function of the calcination temperature is shown in Table 4.4 shows.

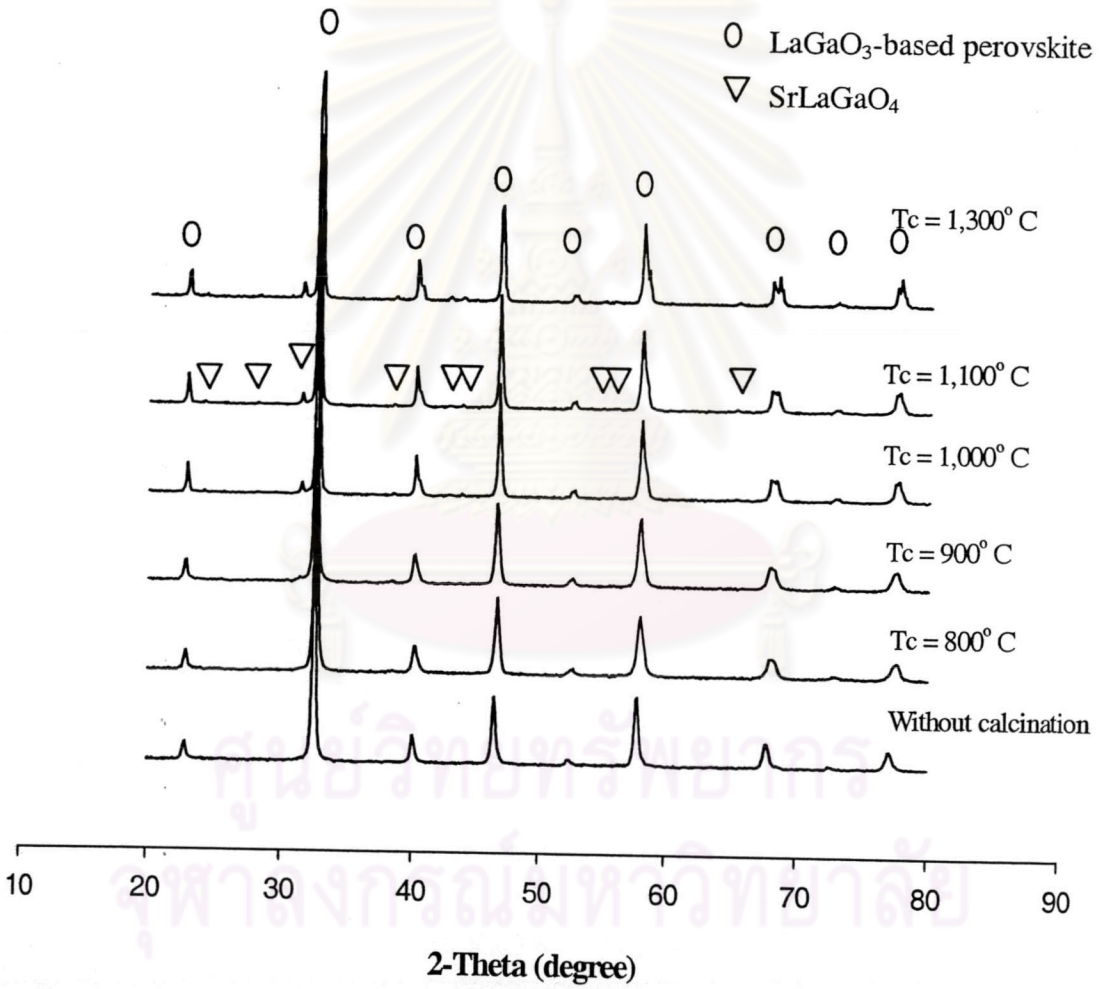

Figure 4.15 XRD patterns of LSGF6428 without and after calcination

According to Figures 4.15 and 4.16, and Table 4.4, the powder calcined at 800-900°C showed a single phase of perovskite cubic structure with no significant change of lattice parameters and weight losses. When the temperatures were higher than 1,000 °C, the asymmetric peaks in the XRD patten were from two phases, in which the phase with a larger lattice had the higher intensity. The lattice parameters were continuously decreasing while the weight losses were increasing as well as the amount of the secondary phase of $SrLaGaO_4$. Previous investigations by many researchers [78, 79, 95] showed that the secondary phase was the result of the volatilization of Ga_2O from the $LaGaO_3$ based perovskite structure. This appears to be consistent with the result of the weight loss osbserved in the present study.

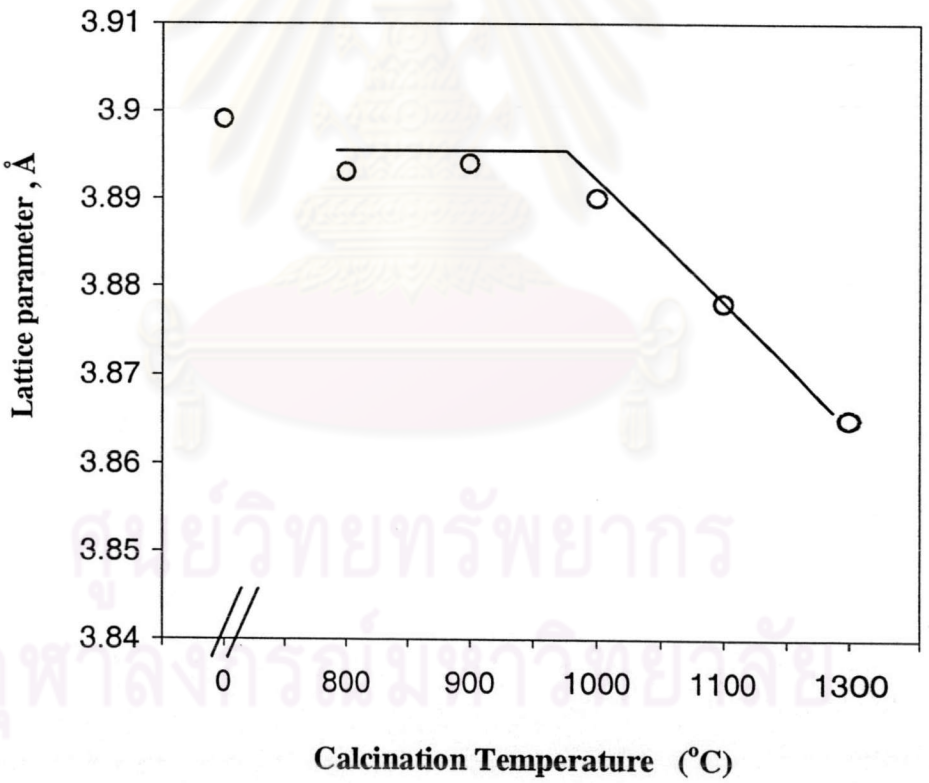

Figure 4.16 Temperature dependence of lattice parameter of LSGF6428 powder

The minor mass loss (0.15 to 0.68%), observed at calcination temperatures between 800-1,100 °C, was probably due to the combustion of the carbon residue. While the mass loss of 1.67%, occurred at 1,300 °C, was due to the volatizaton of Ga_2O as mentioned above. In addition, because we found traces of solid sticking on the alumina crucible, the major loss might also be due, in part, to the melting of $SrLaGaO_4$, which had the melting temperature about 1,400°C [16].

The decrease of the lattice parameter might have come from the consumption of Ga^{3+} (ionic radius 0.62 Å) and Sr^{2+} (ionic radius 1.44 Å) in the formation of the secondary phase. These cations have ionic radii bigger than La^{3+} (ionic radius 1.31 Å) and Fe^{3+} (ionic radius 0.55 Å) that caused the average unit cell parameter to decrease.

Table 4.4 The weight loss of powder at various calcination temperature

Temperature (°C)	Weight of powder (g)		weight loss (%)
	before calcination	after calcination	
800	0.9102	0.9088	0.15
900	0.9702	0.9686	0.16
1,000	0.9647	0.9608	0.43
1,100	0.9565	0.9500	0.68
1,300	0.5545	0.5452	1.67

Therefore it can be concluded that the increase of the calcination temperature did not enhance the single phase of $LaGaO_3$-based perovksite as in $LaCoO_3$-based or barium-containing perovskite. On the other hand, the secondary phase increased with increasing calcination temperature. In the case of single-phase perovskite, the calcination temperature above 1,000°C promoted the secondary phase of $SrLaGaO_4$ with the decrease in lattice parameter.

4.5 The Mechanism of Perovskite Formation

According to the experimental results, the postulated mechanism of perovskite formation was proposed as shown in Scheme 1.

$(1\text{-}x)La(NO_3)_3+xSr(NO_3)_2+(1\text{-}y)Ga(NO_3)_3+yFe(NO_3)_3 + 2HOC(COOH)(CH_2COOH)_2$

$x = y = 0.2\text{-}0.8$

$\downarrow$ 70% HNO_3

Metal-citrate complexes

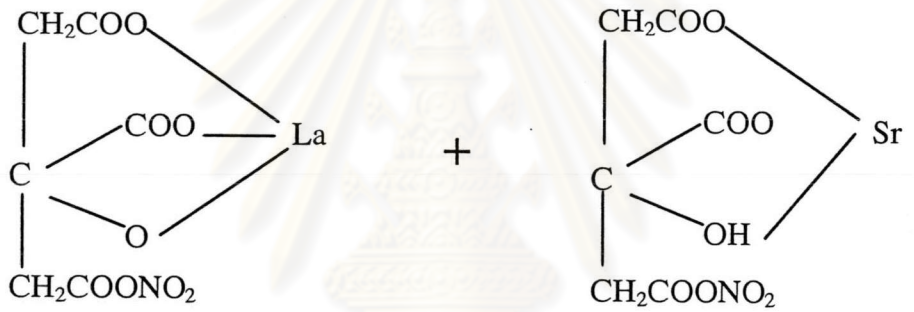

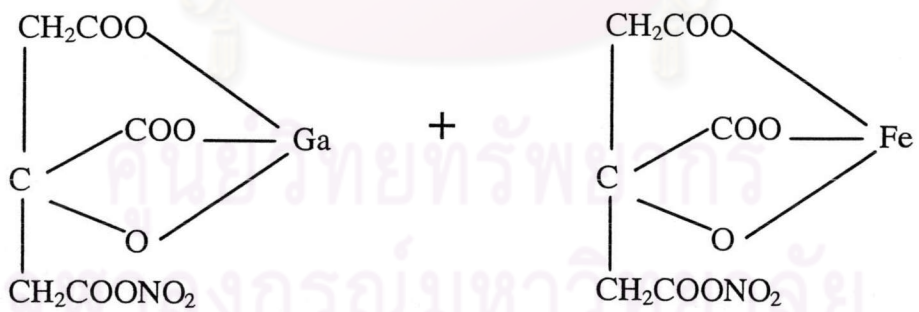

$\downarrow$ NH_4OH

Metal citrate-nitrate gel

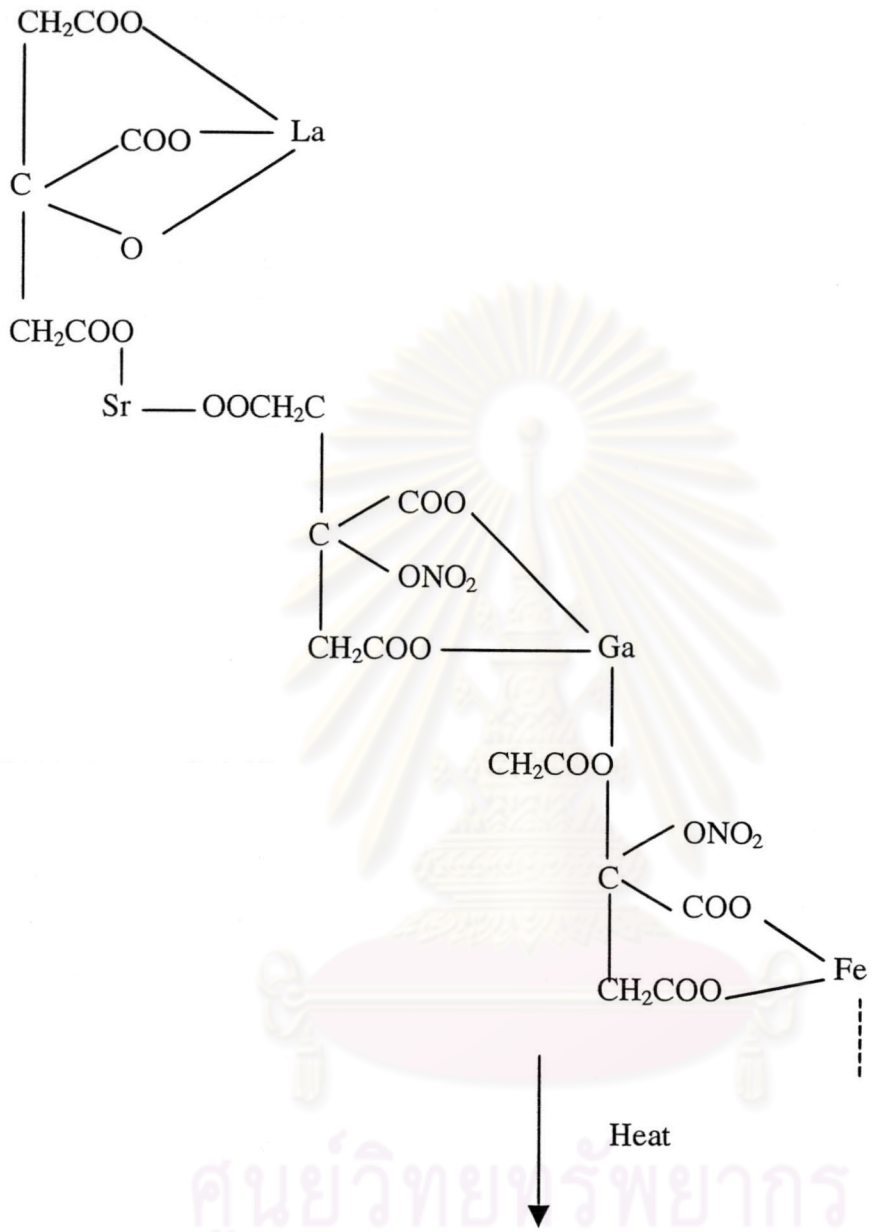

Heat

Evaporation, decomposition, and spontaneous combustion

$$La_{1-x}Sr_x Ga_{1-y}Fe_yO_{3-\delta}\ (s) + 12CO_2\ (g) + 8H_2O\ (g) + 3N_2\ (g)$$

Scheme 1. The posulated mechanism of the formation of perovskite

By modified citrate method, the metal nitrates were dissolved in 70% nitric acid, which then reacted with citric acid to form metal-citrate-nitrate complexes. These metal-citrate complexes could under go polymerization when ammonium hydroxide was added. Meanwhile NH_4OH was added, the white fume of NH_4NO_3 was suddenly observed, which came from the free NO_3^- reacting with NH_4OH and generating the heat. In the case of LSGF6428, the colour of the mixture had been changed from brown to clear brown at pH≈1 and fume stopped at pH≈1. At this point, the remained citric acid and NH_4NO_3 might be dissolved in the solution due to the adding of NH_4OH (10 ml). Then the solution was changed to clear green solution (pH≈1.5) and to green precipitated solution (pH≈3-6). This precipitation indicated the metal citrate-nitrate gel resulting from the polymerization of the metal citrate-nitrate complex when NH_4OH was increased [62]. The solution then changed to clear yellow solution (pH≈7.5) and finally to completely dissolved brown solution (pH≈ 9), which might be because the gel was diluted by the addition of NH_4OH.

The combustion of the metal citrate-nitrate gel solution was composed of three steps, evaporation, decomposition, and spontaneous combustion. The excess solvent was firstly evaporated until a sticky gel was obtained. During the final stage of evaporation, the mixture began to swell, and became viscous. The generated gases could be observed from the large swelling viscous mass. Finally, the spontaneous combustion was initiated by generated gases to convert the mixture to perovskite powder [63]. A typical burning of 40 ml of gel solution was completed within 10 seconds.

Following the previous results, the single-phase perovskite with the fine powder was obtained at pH ≥ 3.39 as revealed. It might be because, at pH = 3.39, all metals in the metal citrate-nitrate gel solution were closed to each other, which could help the transformation to single-phase perovskite at the flame temperature. The increase of pH more than 3.39 did not influence the structure and paricle size of perovskite powder because the metal citrate-nitrate gel was not further polymerized. The additonal NH_4OH was only to dilute the gel. On the other hand, at pH = 1.10, the non-single phase was present because NH_4OH was not enough to polymerize the long chain of metal citrate-nitrate gel. After spontaneous combustion, the short chanin of metal citrate-nitrate gel would be transformed to the secondary phase, $SrLaGaO_4$. In the case of high Ga-containg perovskite, such as LSGF6482, even though the gel was

formed, the non-single phase perovskite was obtained. It was possible that the high Ga-containing gel required higher temperature than the flame temperature to cause phase transform.

4.6 Characterization of the Perovskite Membrane

The synthesized perovskite powder was typically calcined at 900°C for five hours and then pressed into disc. The mixture of wax, polyvinyl alcohol, and polyethylene glycol was added as a binder to improve the shape of perovskite disc. Finally, it was sintered in air at 1,250-1,400 °C for 10-20 hours. It was observed that the membrane was cracked when the rate of heating to the sintering temperature and rate of cooling to the room temperature were at 2 °C/min. Therefore both heating and cooling were performed at a lower rate, 1 °C/min. The structure, densification, and microstructure of each membrane were determined. The influence of sintering temperature and binder addition on the morphology of membrane was also investigated.

4.6.1 Characterization of $La_{0.6}Sr_{0.4}Ga_{1-y}Fe_yO_{3-\delta}$ Membranes

To achieve the dense membrane, the compacting of the perovskite powder and its sintering were important. In most reports, gas pressure bonding or hot isostatic pressing (HIP) was used for preparing the membrane. Such methods utilized a combination of high–pressure inert gas and high temperature to densify the membrane. The other method required organic binder for compacting the powder during pressing. The binders provide lubrication (free flowing) during pressing and give the pressed part enough strength and toughness that can be handled prior to densification [69].

It was reported that the densed LSGF membranes were obtained after sintering at temperature in the range of 1,380-1,600°C for 4-10 hours depending on the composition. The dense LSGF5528 (high Fe content) and $La_{0.8}Sr_{0.2}Ga_{1-y}Fe_yO_{3-\delta}$ where y = 0.2-0.5 (low Fe content) membrane were obtained when sintered at 1,380 and 1,600°C, respectively [9, 10, 13]. In $La_{1-x}Sr_xFeO_{3-\delta}$ compounds, the densed membrane was obtained when sintered at temperature, 1,250 for 4 hours [66]. Accordingly, it seems that the perovskite membrane with the higher Fe content (Ga lean) requires the lower sintering temperature. Generally, the lower sintering temperature requires the longer sintering time to achieve the densed membrane, which has the smaller grain size and vice versa. It was also

reported that the higher Sr content provides the better oxygen permeation and the appropriate amount of Sr was in the range of 0.2-0.4 [10].

Consequently, $La_{0.6}Sr_{0.4}Ga_{1-y}Fe_yO_{3-\delta}$ where y = 0.2, 0.5, and 0.8 membranes were prepared. However, HIP was not available in this laboratory, the membranes were prepared by mixing the perovskite powders and the mixture of PVA 1.5%, PEG1%, and wax 4% by weight of perovskite powder. In general, the non-agglomerated and fine powder enhances the good sinterability, densification at low sintering temperature. Because it is easily to achieve maximum particle packing and uniformity, so that minimum shrinkage, uniform of grain growth, and retained porosity will result during densification [6]. Due to the powder synthesized by the modified citrate method having the smaller average particle size with the less aggregation particles, its membrane might be densed when sintering at the sintering temperature, 1,250°C for a long time, 20 hours.

Figure 4.17 showed the XRD patterns of three $La_{0.6}Sr_{0.4}Ga_{1-y}Fe_yO_{3-\delta}$ membranes where y = 0.2, 0.5, 0.8 after sintering at 1,250°C for 20 hours. All membranes remained cubic structure as shown by the characteristic peaks at 2Θ = 22.5, 32.5, 40, 46, 52, 57.5, 67.5, 77.5 degree. The splitting peaks at 2Θ = 48.1, 58.2, and 67.6 degrees were found in addition to the pattern of $LaGaO_3$-based perovskite in both LSGF6455 and LSGF6482 but not LSGF6428. This indicated the distortion of the cubic structure of LSGF6428 membrane. As perovskite powders, the LSGF6428 membrane still exhibited the single-phase structure while the other membranes showed the presence of the secondary phase of $SrLaGaO_4$ as in Figure 4.8. Therefore it might be said that, even the powder was compacted and heated at the higher temperature than calcination temperature, the phase transformation of non-single phase perovskite to single-phase perovskite was not presented.

The surface and cross section of $La_{0.6}Sr_{0.4}Ga_{1-y}Fe_yO_{3-\delta}$ membranes were investigated by SEM technique as presented in Figure 4.18. All three membranes had average grain diameters of around 1 μm when sintered at 1,250°C. It was confirmed by the results of Beaker et al. [94]. They prepared the three membranes, namely $La_{0.9}Sr_{0.1}GaO_{3-\delta}$, $La_{0.9}Sr_{0.1}Ga_{0.95}Fe_{0.05}O_{3-\delta}$, and $La_{0.9}Sr_{0.1}Ga_{0.8}Fe_{0.2}O_{3-\delta}$ from the corresponding powder synthesized by solid state method. All membranes have average

grain diameters of around 1 μm after sintering at 1,500°C [94]. Therefore the Fe content in the perovskite powder had no influence on the grain size of membrane after sintering.

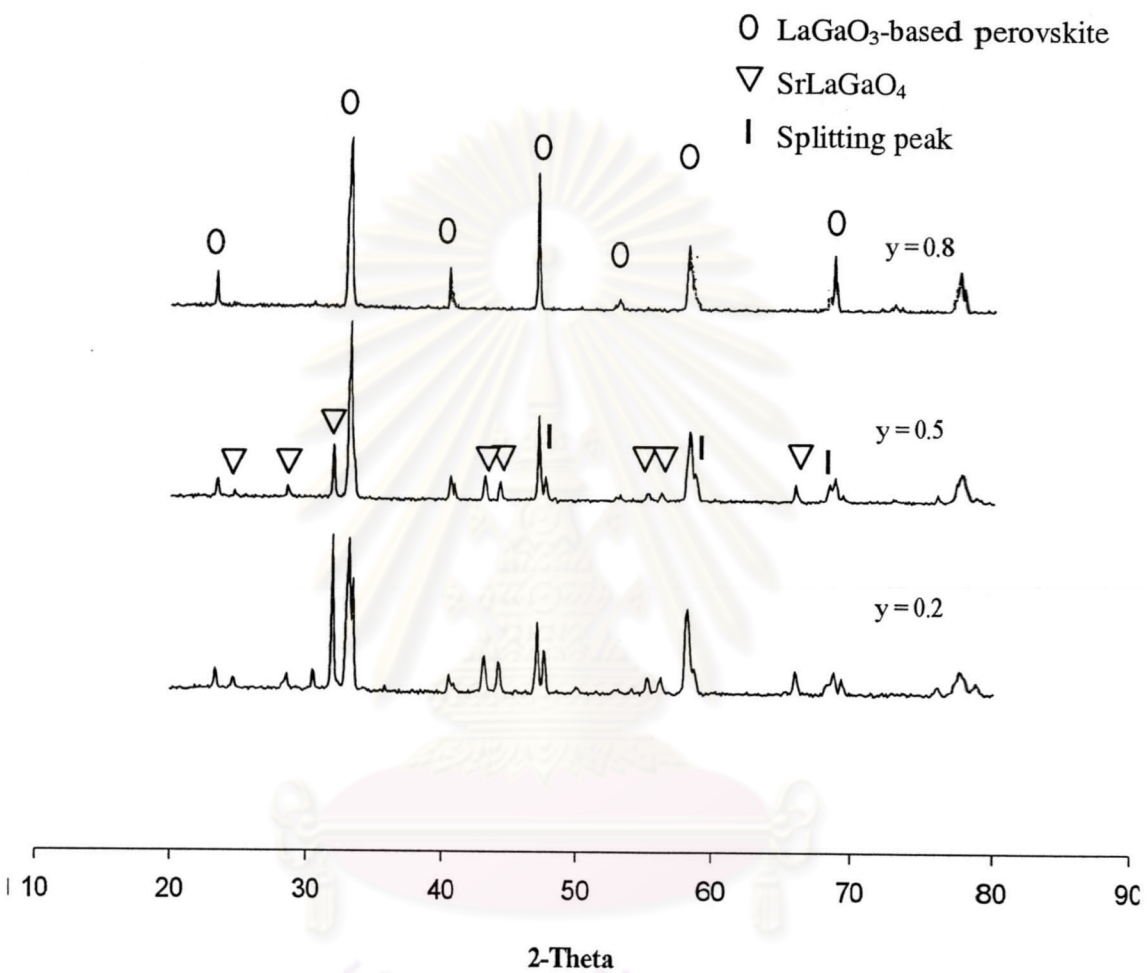

Figure 4.17 XRD patterns of the $La_{0.6}Sr_{0.4}Ga_{1-y}Fe_yO_{3-\delta}$ membranes (y = 0.2, 0.5, 0.8) after sintering at 1,250°C for 20 hours

The morphology of grains of membranes was also considered. All membranes also showed the intermediate stage during which the necks become large, resulting in the formation of an interconnected pore structure. In Figure 4.18 (a, b), SEM showed the spherical morphology of grains of LSGF6428 membrane whereas the other SEM pictures, Figure 4.18 (c-f), showed the other shape, needle shape, lying on the matrix surface and cross section of LSGF6455 and LSGF6482 discs. The characterization of the

needle shape should be further studied. However, it might be due to the presence the secondary phase of $SrLaGaO_4$, which appears on the perovskite structure. This was supported by the results of Beaker et al [94]. They reported the two other phases lying on top of the Sr- and Fe- doped perovskite membranes. These were vitreous plates, which had the appearance of a solidified liquid, and needle-shaped crystals, which appeared to have crystallised from this liquid phase. After characterization, these phases contained La, Sr, and Ga.

The densification of all membranes was studied. The relative densities were calculated from the bulk density divided by the theoretical density as described in section 3.3.4. Generally, to complete the densification of the membrane, the percentage of relative density should be higher than 90% [68, 69]. For synthesized $La_{0.6}Sr_{0.4}Ga_{1-y}Fe_yO_{3-\delta}$ membranes where y = 0.2, 0.5, and 0.8, the relative densitiy was about 69, 72, and 80%, respectively. The lower relative density than 90% and the observation of the interconnected pore (diameter < 1 μm) suggested that the densification of samples was not complete after sintering at 1,250°C for 20 hours. The undensed membranes were obtained even though the long sintering time, 20 hours, was used. Therefore, the sintering temperature should be increased above 1,250°C to complete the densification. The XRD analysis showed that there was no change in the perovskite structure during the membrane preparation step. The LSGF6428 membrane exhibited the single-phase perovskite structure while the other membranes showed the presence of the secondary phase of $SrLaGaO_4$. Besides, the low sintering temperature and the use of high amount of binder, especially 4% wt of wax, might have caused the low density due to the presence of open pore with the diameter about 3-5 μm as shown in Figure 4.18(d and f). These pores might be resulted from the decomposition of the high molecular weight wax and could not be eliminated at the low temperatures.

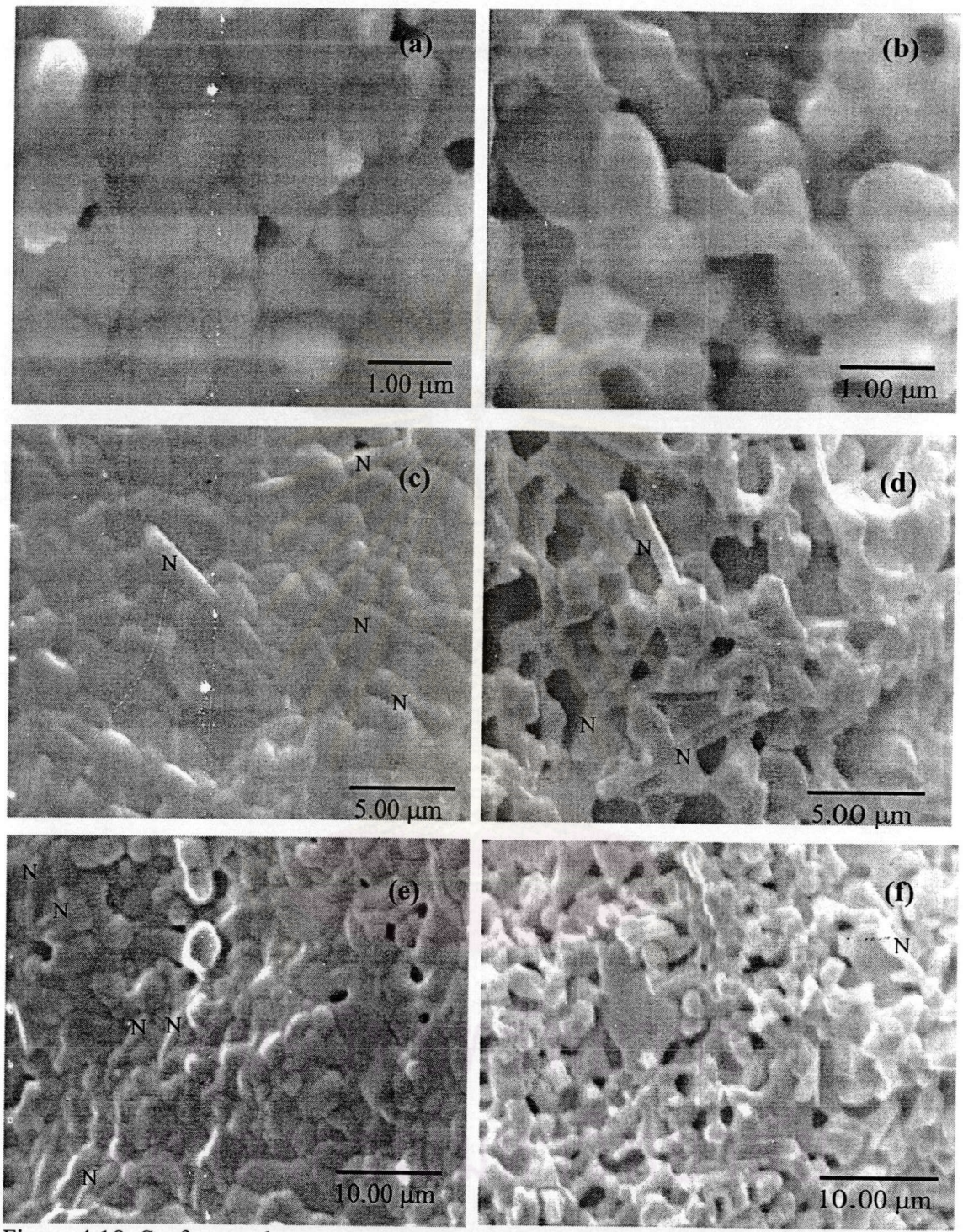

Figure 4.18 Surface and cross section of LSGF membranes sintered at 1,250°C

(a) surface LSGF6428 membrane; (b) cross section of LSGF6428 membrane;

(c) surface LSGF6455 membrane; (d) cross section of LSGF6455 membrane;

(e) surface LSGF6482 membrane; (f) cross section of LSGF6482 membrane

4.6.2 Microstructure of Membranes

The microstructure of membranes at different composition of Sr in $La_{1-x}Sr_xGa_{0.2}Fe_{0.8}O_{3-\delta}$ and $La_{1-x}Sr_xGa_{0.4}Fe_{0.6}O_{3-\delta}$ was studied by SEM as shown in Figure 4.19 and 4.20, respectively. From the previous section, the results indicated that the undensed membrane was obtained due to the low sintering temperature and the use of binder. However, to form the disc shape, the binder still was used. Therefore, all samples were prepared from calcined powder mixed with wax 2%, polyvinyl alcohol 1%, and polyethylene glycol 1%. The green discs were sintered at 1,380°C for 10 hours as Ming et al [13]. The SEM micrographs were used to calculate the average grain size of the particles in each case.

In Figure 4.19, SEM micrographs of unpolished-surface membranes clearly showed that the grain size increased from 1, 2, and 5 μm with increasing Sr content in $La_{1-x}Sr_xGa_{0.4}Fe_{0.6}O_{3-\delta}$ where x = 0.2, 0.4, and 0.6, respectively. The grain growth phenomenon was supported by the results from SEM micrographs of cross section of $La_{1-x}Sr_xGa_{0.2}Fe_{0.8}O_{3-\delta}$ membranes, shown in Figure 4.20. The average grain size was about 5 μm for LSGF6428 membrane while the loose interconnectivity of grain was observed from the higer Sr content membrane, LSGF4628 membrane. The average grain size, developing with Sr content, should indicate that the doped Sr in $LaGaO_3$ decreased the sintering temperature. This means, at the same sintering temperature, the bulk density of membrane would be increased with the amount of Sr. The similar phenomenon was observed by several other researchers [75, 76]. Kleveland et al [75] found the grain growth from the Ca or Sr substituted $LaCoO_3$-based perovsktie membranes. The powders were prepared from nitrate precursors using the glycine-nitrate and the EDTA method. The densification of these membranes is shifted to lower temperatures when $LaCoO_3$ is substituted by Sr or Ca. M. Mori et al [76] studied the bulk densities of the $La_{1-x}Sr_xCrO_3$ membranes, whose the powders were synthesized by solid state method, after sintering at 1,600°C for 10 hours. The results also showed that the bulk density increased with increasing Sr content. It was also reported that the heavy doping causes a large thermal expansion under a reducing atmosphere, therefore, the Sr-dopant content in the

lanthanum chromites was significantly limited [76]. However, Sr doping was also indispensable in obtaining a dense lanthanum chromite body.

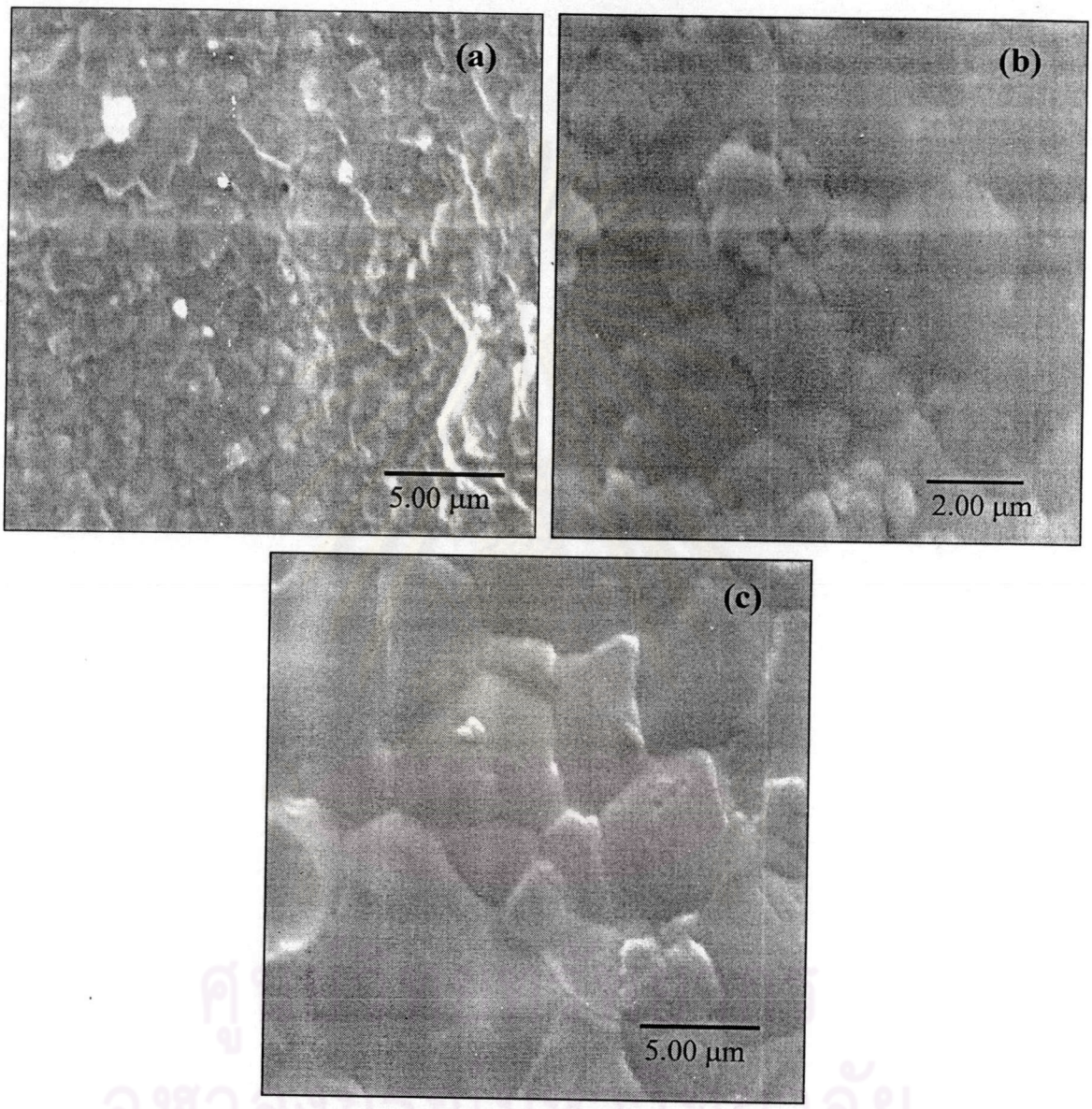

Figure 4.19 Unpolished surface of $La_{1-x}Sr_xGa_{0.4}Fe_{0.6}O_{3-\delta}$ samples sintered at 1,380°C for 10 hours: (a) x = 0.2 (b) x = 0.4 (c) x = 0.6

As seen in Figure 4.20, the membrane should be in the final sintering stage because the pores became isolated and the interconnectivity of pores were eliminated [70, 71]. Eventhough the cross section of LSGF4646 membrane was not characterized,

its grain size equal to the grain size of LSGF6428 (5 μm) would indicate that this membrane was also in the final stage of sintering. Therefore, the LSGF4646, LSGF6428 and LSGF4628 membranes should be densed when sintered at 1,380°C. However, the large open pores (10 μm) indicated the undensed membranes. These pores might be resulted from the decomposition of wax. Because of the large molecular weight of wax, the pores could not be eliminated even though the membranes were sintered at high temperatures.

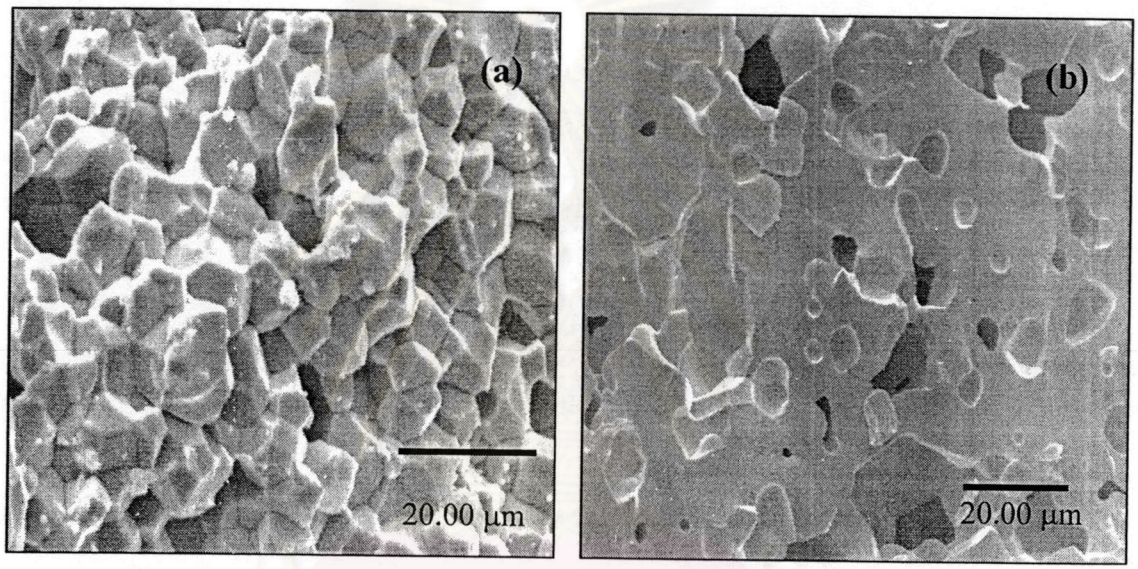

Figure 4.20 Cross section of $La_{1-x}Sr_xGa_{0.2}Fe_{0.8}O_{3-\delta}$ samples sintered at 1,380°C for 10 hours: (a) x = 0.4 (b)x = 0.6

Following our results and references, the substitution of Sr in $LaGaO_3$ decreased the sintering temperature due to the grain growth in the samples with higher Sr content. The LSGF4646, LSGF6428 and LSGF4628 membranes were in the final stage of sintering at 1,380°C but these membranes were not dense due to the use of binder. On the other hand, the grain growth phenomenon was not found when the Fe content was increased. The grain size with a diameter around 1 μm was observed in all $La_{0.6}Sr_{0.4}Ga_{1-y}Fe_yO_{3-\delta}$ membranes.

Therefore, the influence of sintering temperature and binder on the morphology of membranes should be further studied.

4.6.3 The Influence of Sintering Temperature on the Morphology of $La_{0.6}Sr_{0.4}Ga_{0.2}Fe_{0.8}O_{3-\delta}$ Membranes

Since LSGF6428 melted at 1,400°C, its membrane was sintered at the temperature from 1,250 up to 1,380 °C. Three membranes prepared without binder sintered at 1,250-1,380°C were characterized by XRD as shown in Figure 4.21.

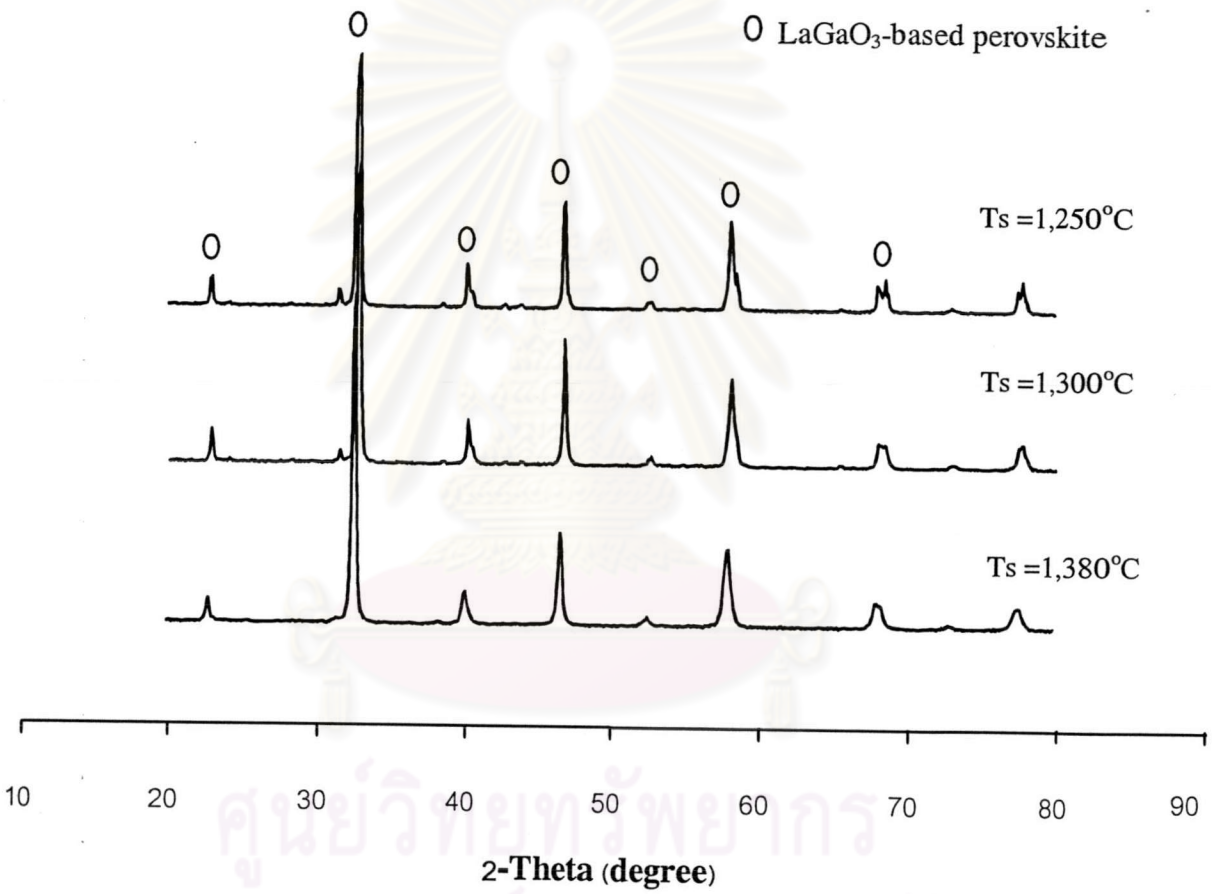

Figure 4.21 XRD patterns of LSGF6428 membranes sintered at different temperatures for 10 hours

The peaks of each sample can be clearly indexed at 2Θ of 22, 32, 40, 46, 53, 57, 68, 74, and 77 degrees and no impurity peaks were observed, indicating the membranes prepared by the modified citrate method were most likely single phase with cubic perovskite structures.

SEM of the surface and cross-section of the LSGF6428 samples, which had been sintered at 1,250 and 1,380°C were shown in Figure 4.22. The average grain size of both samples was 1μm and 4 μm, respectively. The results clearly demonstrated the sintering temperature affected the grain size. After sintering at 1,250°C many closed pores were still observed as expected from the densification property which exhibited the incomplete densification at the relative densities of 80%. The grain size and density of the samples increased steadily with increasing sintering temperature. When sintered at 1,380°C, the materials became dense due to the grain growth (5 μm) and closed pore which indicated the final sintering stage and due to the relatively densities of 95% which implied the completely sintering.

According to the XRD pattern, SEM, and the relative density, it could be concluded that the membranes prepared without binder having the single-phase perovskite structure were successfully densed under sintering condition, 1,380°C for 10 hours.

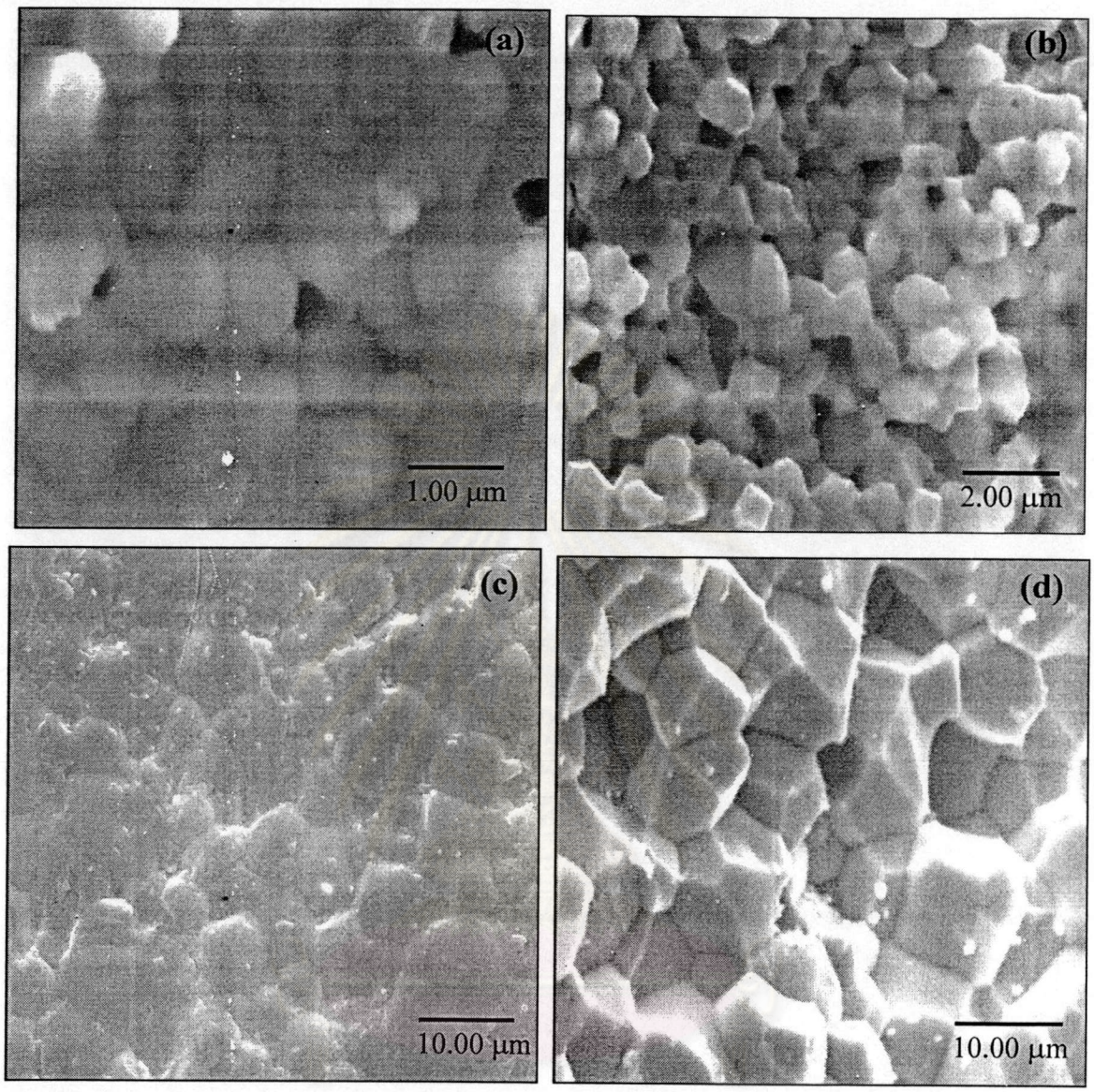

Figure 4.22 SEM pictures of surface and cross section of LSGF6428 membranes sintered at different temperature for 10 hours

(a) surface membrane sintered at 1,250°C;

(b) cross section of membrane sintered at 1,250°C;

(c) surface membrane sintered at 1,380°C;

(d) cross section of membrane sintered at 1,380°C

4.6.4 Characterization of $La_{0.4}Sr_{0.6}Ga_{0.4}Fe_{0.6}O_{3-\delta}$ Membranes

According to the results from section 4.4.2 and 4.4.3, LSGF4646 membrane prepared without binder was sintered at 1,380°C for 10 hours. The XRD pattern of the membrane was shown in Figure 2.23. Due to the observation of the characteristic peaks of $LaGaO_3$-based perovskite structure and the low intensity of impurity peak ($2\Theta = 30$ degree), this indicated that the membrane was most likely single phase with the cubic perovskite structures. After sintering at 1,380°C, the membrane had the relative density more than 90%.

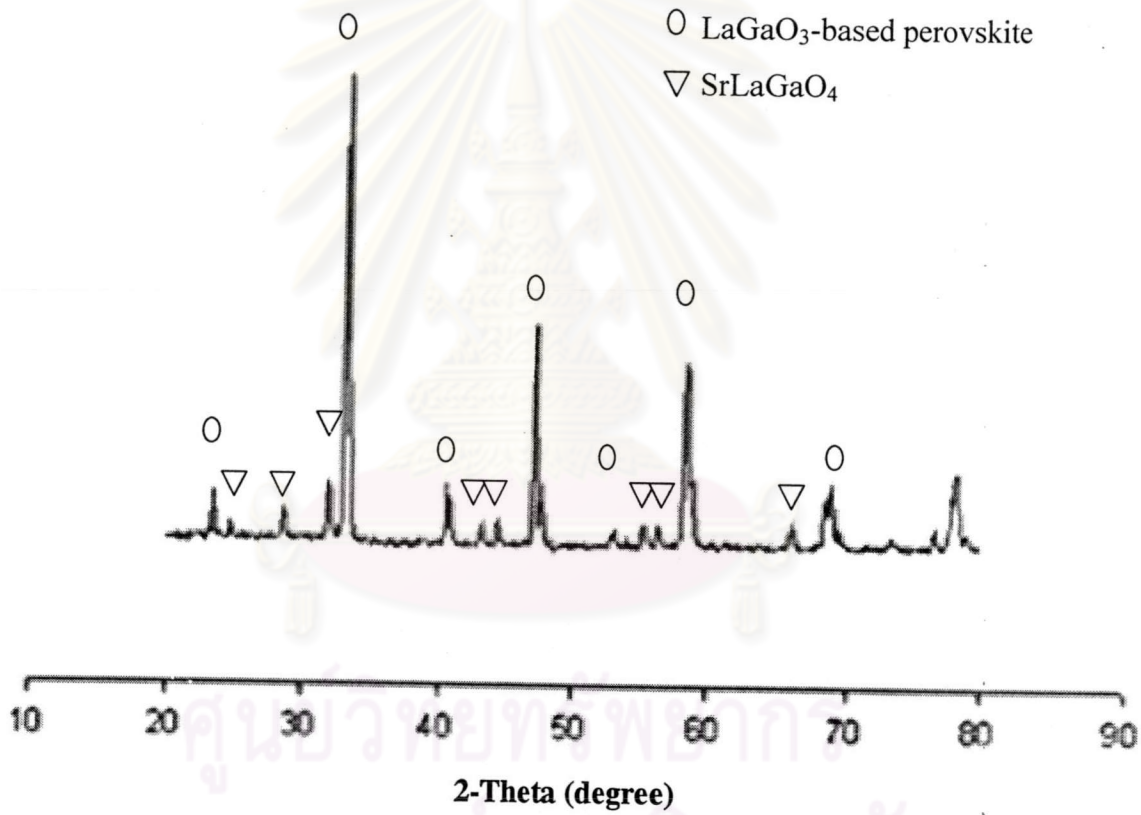

Figure 4.23 XRD patterns of LSGF4646 membrane sintered at 1,380°C for 10 hours

According to the SEM (Figure 4.19), the XRD pattern (Figure 4.23), and the relatively density, it can be concluded that the LSGF4646 membrane prepared without binder having the single-phase perovskite structure was successfully densed under sintering condition, 1,380°C for 10 hours.

4.6.5 The Influence of Binder on the Morphology of LSGF6428 Membranes

Even though the membrane with the relative density over 95% was obtained after sintered above 1,350°C, the preparation of membrane without binder was hardly used. The spring back effect was appeared on membrane without binder.

Normally, a pore-free ceramic membrane can be made by one of the following methods to carry out the sintering process successfully, to apply an extremely high temperature, to control the distribution of particle diameter, to use an additive such as poly(vinyl alcohol), poly(ethylene glycol), and wax, to utilize a chemical reaction, to employ HIP (hot isotropic pressing), hot pressing, or molten particle deposition [74]. Generally, the use of HIP is the best way to obtain the pore-free membrane due to the good compacting with no need of a binder. However, in this work, the use of a binder was chosen to obtain a perfect membrane because there was no available instrument.

To enhance the compaction, the iso-propanol was used to disaggregate the powder before pressing. The temperature was set at as high as possible, which was 1,380°C. The LSGF6428 membrane was prepared by mixing perovskite powder with binding agents, i.e. the mixture of 1.5% poly(vinyl alcohol) (PVA), 1% poly(ethylene glycol) (PEG), and 4% wax. Then the membrane was sintered at 1,380°C for 10 hours.

As shown in Figure 4.24 (a,b), it was obvious that the membrane contained the open pore with the diameter about 10 μm inside the disc even though the SEM picture showed the densed surface. This pore came from the combustion of the binder which generated CO_2 and H_2O evaporating to the surface. Although the sintering temperature was kept at 600 °C for 1-2 hours before heated to desire sintering temperature, the open pore still remained. Normally, these pores should sinter together, when the temperature was risen to sintering temperature. It might be because the high amount of the high molecular weight wax was used as a binder. This is substantiated by the SEM pictures of membrane cross section in Figure 4.24 (c, d). For sintered membrane without binder at 1,250°C for 10 hours, the cross section of membrane contained the small pore with the diameter less than 1 μm which should be closed when the temperature was increased.

These results showed that when the binder was used, the large pore in the membrane was developed, which could not be sintered even high temperature was used. Therefore the appropriate amount of binder should be determined in further study.

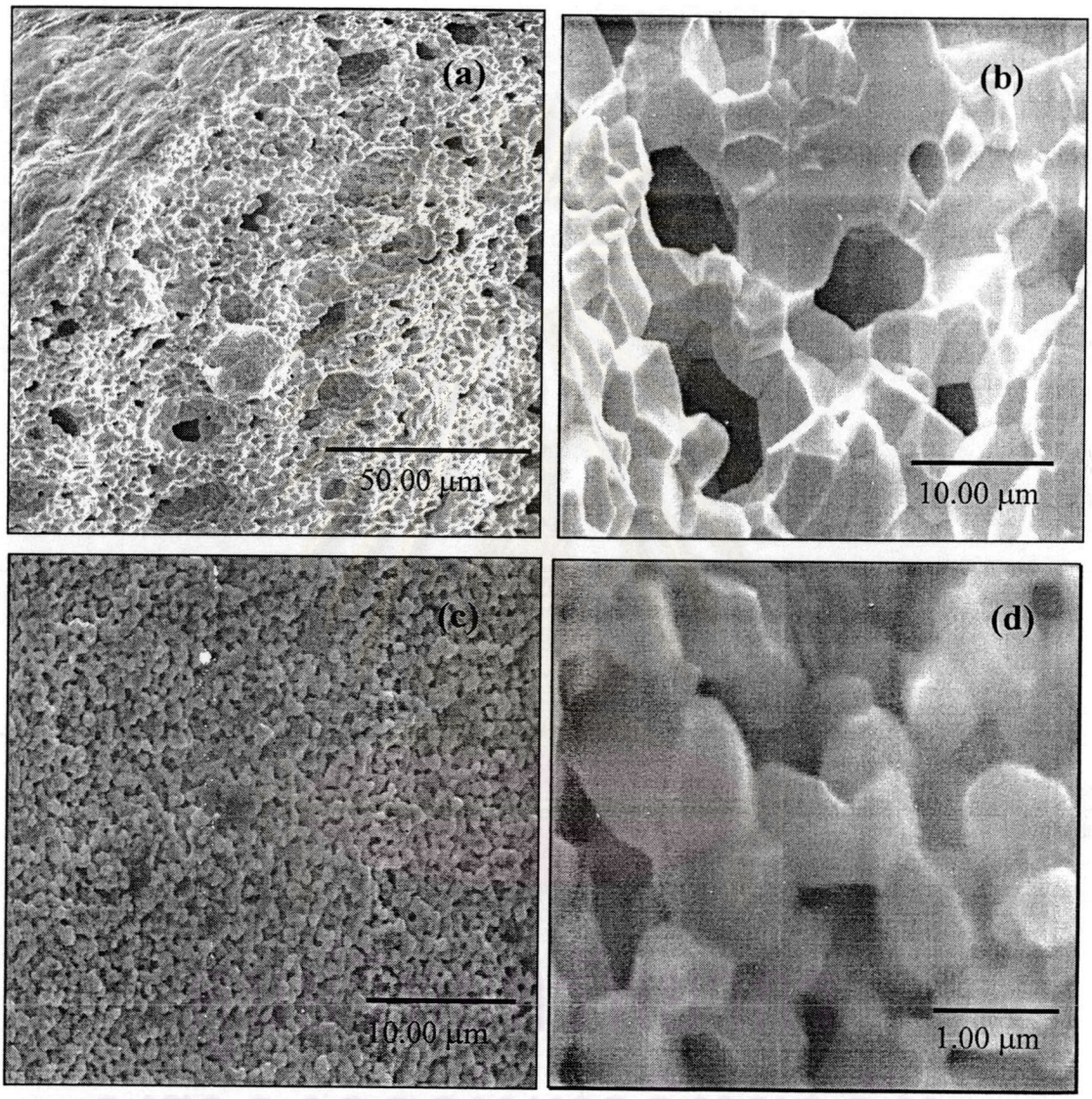

Figure 4.24 Cross Section of LSGF6428 Membranes

(a) and (b) with binder and sintered at 1,380°C, x 1500 and x 10000, respectively;

(c) and (d) no binder and sintered at 1,250°C, x 2500) and x 15000, respectively

4.6.6 Summary of Characterization of the Perovskite Membranes

The membranes were prepared by pressing the powders using a uniaxial pressing machine to form a disc (13 mm diameter, 1 mm thickness) and sintering at 1,250-1,380°C for 10 hours. These membranes were characterized by studying the structure, densification, and microstructure. The substitution of Sr in $LaGaO_3$ decreased the sintering temperature due to the grain growth in the membrane with higher Sr content, while this phenomena was not found when the amount of Fe was increased. All the different Fe containing membranes had average grain diameters of around 1 μm when sintered at 1,250°C. The phase transformation to the single-phase perovskite of membrane was not enhanced by the sintering temperature. The densification of samples was not completed after sintering at 1,250°C. The LSGF6428 and LSGF4646 membranes prepared without binder having the single-phase perovskite structure were successfully densed under sintering condition, 1,380°C for 10 hours.

When the sintering temperature were increased above 1,350°C, the densification of samples was nearly complete with the relative density over 95%. The membranes remained the cubic structure under the sintering temperature below 1,400°C.

The spring back effect appeared on membrane without binder, therefore the use of binder was necessary. However, this caused the large pore inside the membranes, which could not be sintered at high temperature. Therefore the appropriate amount of binder should be further studied.

4.7 Oxygen Permeation of $La_{0.6}Sr_{0.4}Ga_{0.2}Fe_{0.8}O_{3-\delta}$ and $La_{0.4}Sr_{0.6}Ga_{0.4}Fe_{0.6}O_{3-\delta}$ membranes

The oxygen permeation of LSGF6428 and LSGF4646 membranes was determined at 900°C. Before starting the experiment, helium was flushed into the permeate side of the reactor to replace air completely which was monitored by GC. During the oxygen permeation testing, the membrane disc was exposed to the air on the feed side and pure helium on the permeate side with the flow rate of 150 and 30 cm^3/min respectively (Figure 3.2.). Then the gas mixture on the permeate side was analyzed for the individual gas presented in the mixture.

4.7.1 $La_{0.6}Sr_{0.4}Ga_{0.2}Fe_{0.8}O_{3-\delta}$ membrane

Although the LSGF6482 membrane with 0.58 mm thickness had the relative density 80%, indicating the incomplete densed membrane, its oxygen permeability was investigated. During the reactor assembly as described in section 3.2, the nitrogen was flowed into the feed side of the reactor from time to time and checked for the amount of detected nitrogen from the permeate side. The same amount of nitrogen detected by gas chromatography indicated the complete sealing.

Each highly purified gas, helium, nitrogen, or oxygen was passed into the feed side of the reactor at the flow rate of 150 ml/min. Then the pressure was adjusted by using pressure valve until it was increased to the desired pressure difference between feed side and permeate side of the reactor ($\Delta P = P_{inlet} - P_{atm}$). The flux of each gas was measured from the flow rate of permeated gas at 900°C as shown in Figure 4.25. The flux increased with increasing ΔP, which was a driving force of permeation. It was found that the experimental assembly could stand at temperature 900°C and the pressure difference between feed and permeate sides up to 0.4 atm.

Oxygen exhibits the highest flux among three gases while helium shows a slightly higher flux than nitrogen. If the membrane were densed and gas-tight, the direct passage of every gas molecule would be blocked. Only the oxygen ions can migrate selectively through the mixed ionic and electronic conductivity membrane. Dissociation and ionization of oxygen occurred at the oxide surface at the high-pressure side (feed side, P'_{O_2}), where electrons are picked up from accessible (near-) surface electronic states.

Upon arrival at the low-pressure side (permeate side, $P''o_2$), the individual oxygen ions with their electrons recombined again to form oxygen molecules, which are released in the permeate stream. In the case of helium and nitrogen, both gases could not receive electron and were not able to permeate. Therefore, in this experiment, the observation of the flux of helium and nitrogen indicated that these gases diffuse through the pore inside the membrane. Because the lower molecular weight of gas would diffuse faster than the higher one, the higher flux of helium than nitrogen was also confirmed the diffusion of gas. Even though oxygen can diffuse through the undense membrane, the highest flux of oxygen with the highest molecular weight among three gases indicated that oxygen mostly permeated from the membrane by dissociation and ionization. Therefore, it could be said that the LSGF6428 membrane could be used as membrane for separation of oxygen from nitrogen.

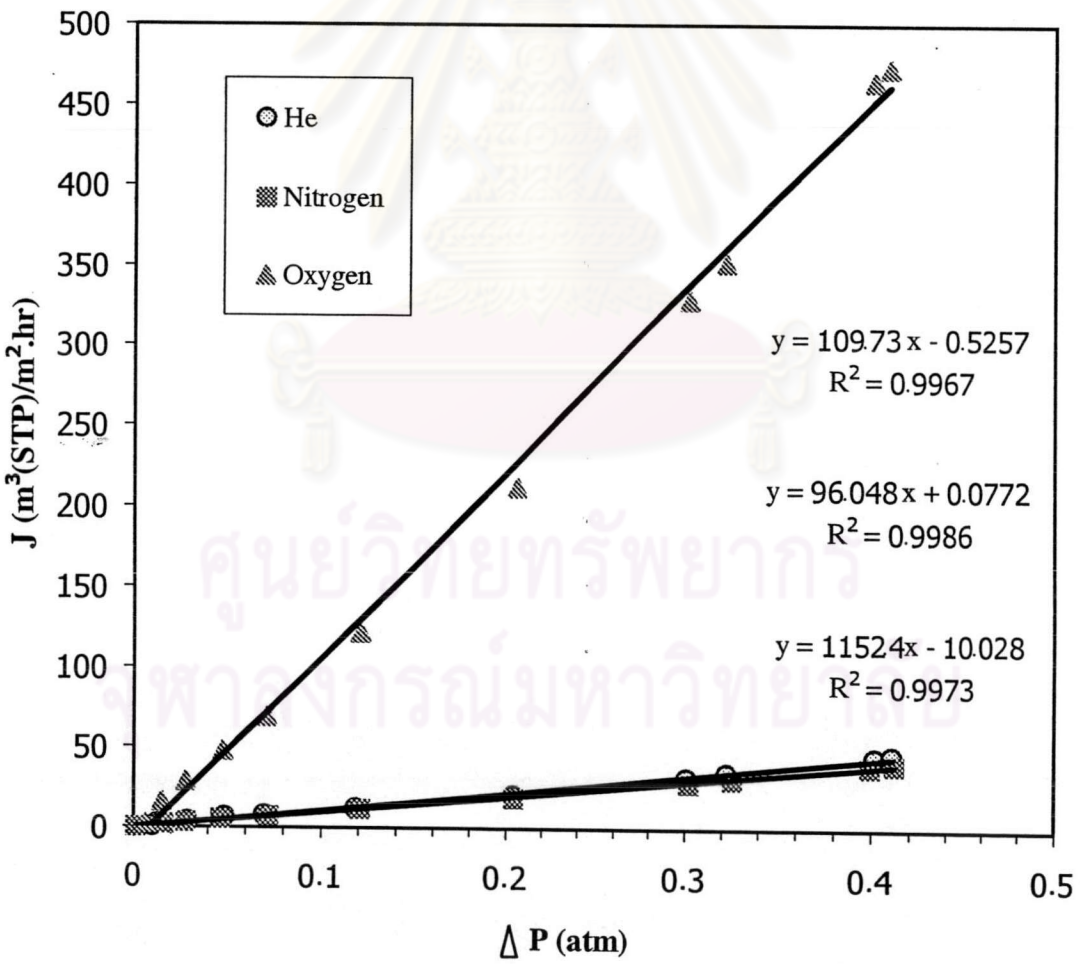

Figure 4.25 Flux of each gas at different ΔP

The membrane was then used for separation of oxygen from air. Figure 4.26 shows the efficiency of oxygen separation from air during the permeation run by using LSGF6428 membrane.

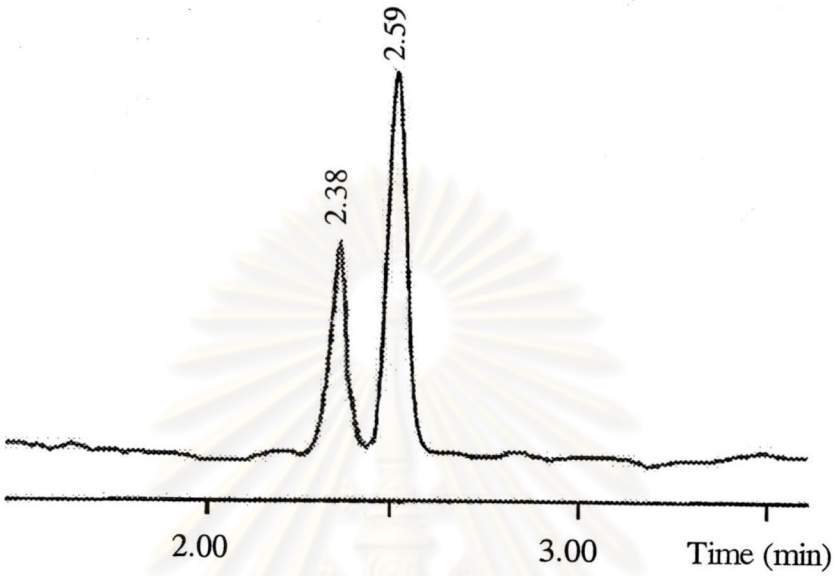

Figure 4.26 Gas Chromatogram from an oxygen permeation experiment through LSGF6428 membrane

The oxygen and nitrogen were observed at retention time, 2.38 and 2.59 minutes, respectively. The percentage of permeated oxygen from air is shown in Figure 4.27.

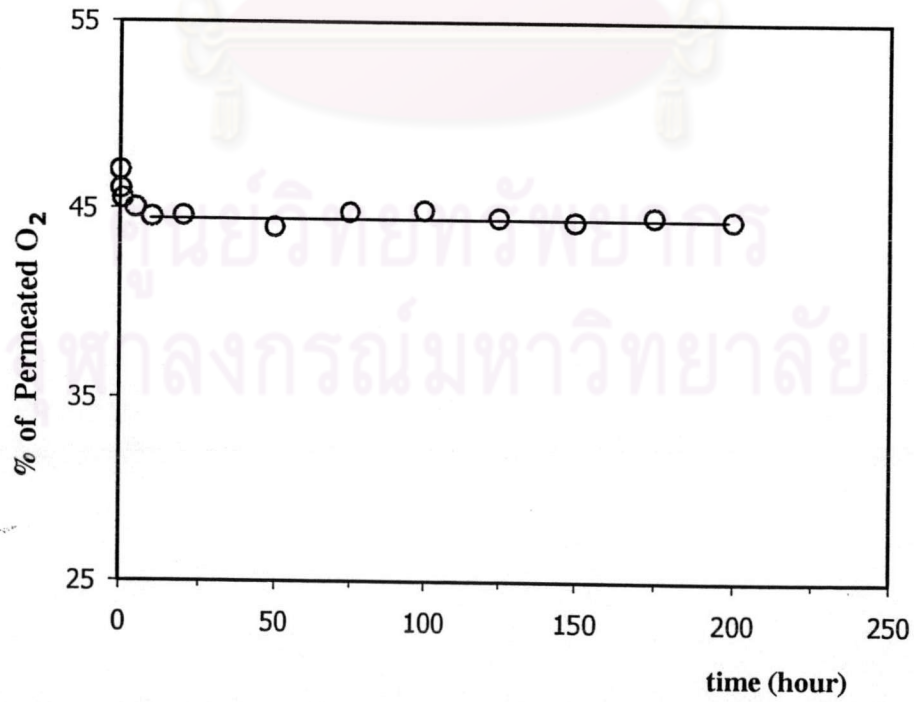

Figure 4.27 The percentage of permeated oxygen as a function of time at 900°C

Due to the permeation of oxygen and the diffusion of oxygen and nitrogen on the undensed LSGF6428 membrane, instead of oxygen permeation flux, the percentage of permeated oxygen was measured. By the GC external standard method, the percentage of permeated oxygen was calculated from the deduction of the total concentration of oxygen with the concentration of diffused oxygen (0.21/0.79 x concentration of diffused nitrogen) divided by the sum of total concentration of oxygen and nitrogen. Figure 4.27 shows the percentage of permeated oxygen as a function of time at 900°C.

As shown in Figure 4.27, after the sealing procedure had proceeded, gas streams were passed through the membrane surfaces. The ratio of oxygen permeation, starting at a much higher value, decreases with time and eventually levels off. This might be due to the lessening of surface oxygen desorption rates and the readjusting of the lattice parameters as reported by several groups [51, 56, 80]. The percentage of oxygen was decreased from 47% to the steady-state value of 44% in 15 hours. Even though the undensed membrane was used, it can be seen that the LSGF6428 membrane could enrich the oxygen in air up to 45% and was stable for the long time permeation.

4.7.2 $La_{0.4}Sr_{0.6}Ga_{0.4}Fe_{0.6}O_{3-\delta}$ membrane

For a complete densified LSGF4646 membrane (0.62 mm thickness) with a perfect seal, the separation efficiency for oxygen from air is 100%. Figure 4.28 shows an example of 100% O_2 selectivity for the separation of oxygen from air in a helium/air

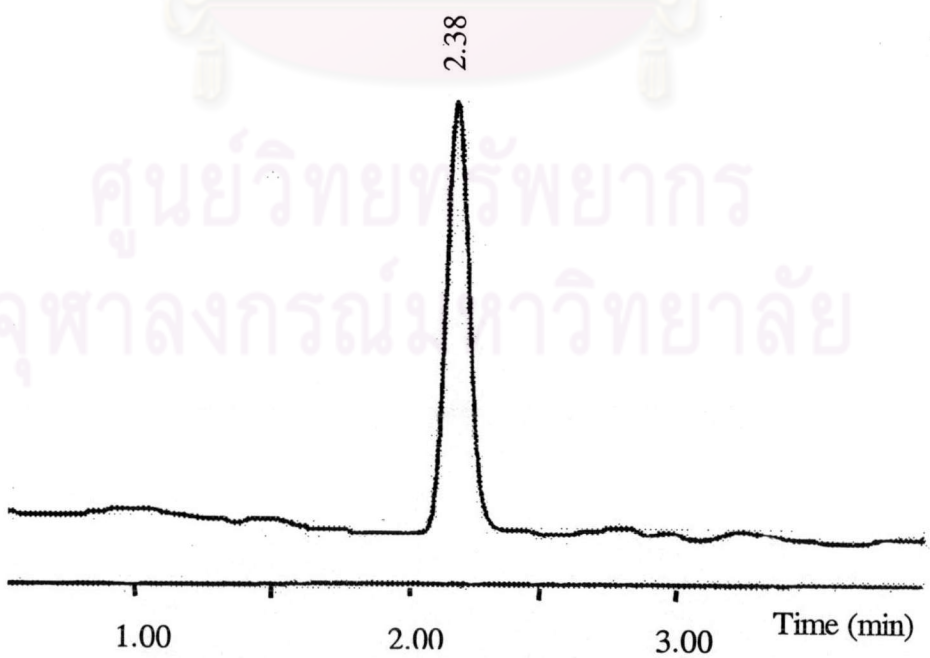

Figure 4.28 Gas Chromatogram of the permeated gas through LSGF4646 membrane

gradient. Oxygen flux was near 0.1 cm^3 (STP)/min/cm^2. A single oxygen peak was at retention time, 2.38 minute, in the chromatogram. The nitrogen peak was below the detectable level by the high sensitivity TCD detector.

The oxygen permeation rates for LSGF4646 membrane compared with membranes from the other reports is shown in Figure 4.29. Experimental data in Figure 4.29 were correlated to the equation indicated in Appendix B.

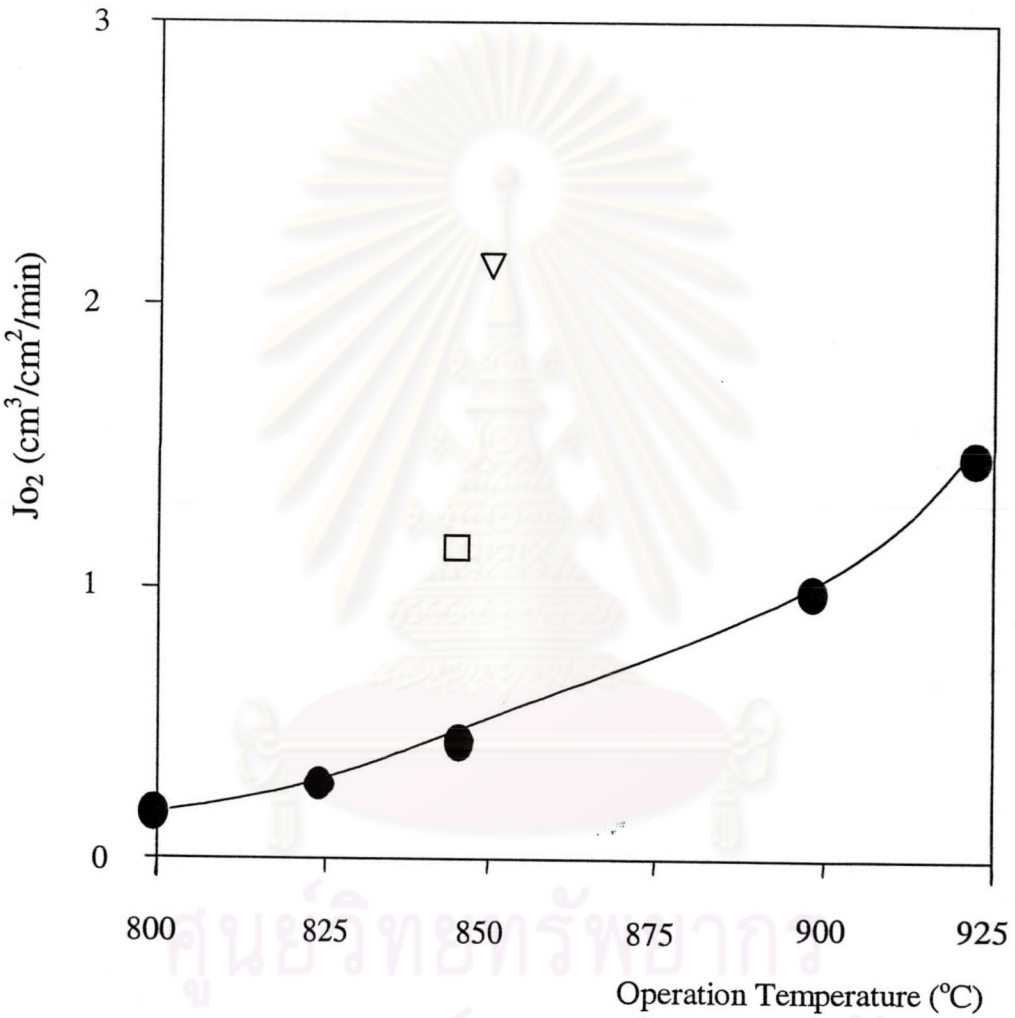

Figure 4.29 Temperature dependence of oxygen permeation rate for LSGF4646 membrane
(●) our study ($La_{0.4}Sr_{0.6}Ga_{0.4}Fe_{0.6}O_{3-\delta}$, 0.62 mm);
(□) Yang et al. (2001) ($Ba_{0.5}Sr_{0.5}Co_{0.8}Fe_{0.2}O_{3-\delta}$) [51];
(▽) Tasi et al (1998) ($La_{0.6}Ba_{0.4}Co_{0.8}Fe_{0.2}O_{3-\delta}$, 0.55 mm) [56].

Oxygen permeation could be observed at temperatures higher than 800°C, and the fluxes increased with an increase in temperature. The oxygen flux of 1.5 $cm^3(STP)/cm^2.min$ was achieved at 925 °C. It was reported that oxygen permeation rate of $Ba_{0.5}Sr_{0.5}Co_{0.8}Fe_{0.2}O_{3-\delta}$ $La_{0.7}Sr_{0.3}Ga_{0.6}Fe_{0.4}O_{3-\delta}$, and $La_{0.6}Ba_{0.4}Co_{0.8}Fe_{0.2}O_{3-\delta}$, was 1.1 (at 850°C), 1.8 (at 1000°C), and 2.1 (at 854°C) $cm^3(STP)/cm^2.min$, respectively, under similar condition [13, 51, 56].

Considering the oxygen permeating rate of 1.5 $cm^3(STP)/cm^2.min$ at 925°C, it can be said that LSGF4646 membrane exhibited a high oxygen permeation rate and this LSGF might be promising as an oxygen separation membrane.